Modelling Late Toxicity in Hypofractionated Radiation Therapy

Development of Methods and Applications to Clinical Data

Niclas Pettersson

UNIVERSITY OF GOTHENBURG

Department of Radiation Physics, University of Gothenburg

Gothenburg, Sweden 2013

Doctoral Thesis, 2013
Department of Radiation Physics
University of Gothenburg
Sahlgrenska University Hospital
SE-413 45 Göteborg
SWEDEN

ISBN: 978-91-628-8647-9
E-publication: http://hdl.handle.net/2077/32036
Printed in Sweden by Kompendiet

Datta: what have we given?
My friend, blood shaking my heart
The awful daring of a moment's surrender
Which an age of prudence can never retract
By this, and this only, we have existed
Which is not to be found in our obituaries
Or in memories draped by the beneficent spider
Or under seals broken by the lean solicitor
In our empty rooms

T.S. Eliot, The Waste Land (1922)

ABSTRACT

In hypofractionated radiation therapy (RT), the treatment is delivered by few fractions with high doses per fraction. This is in contrast to conventionally fractionated RT where the total dose is delivered in many fractions with low doses per fraction. Hypofractionation is increasingly used in RT for small tumour volumes, but knowledge about radiation-induced toxicity in healthy tissue (organs at risk, OARs) and suitable methods for modelling toxicity in this specific situation is limited. The aim of this thesis is to investigate radiation-induced toxicity in normal tissue caused by hypofractionated RT through the development of modelling methods and their applications to clinical data. Particular emphasis will be on the fractionation effect.

The thesis treats theoretical and practical aspects of normal tissue complication probability (NTCP) modelling such as radiobiologically consistent dose-response curves, how to estimate composite doses in combined radiation therapy with limited treatment information and how to manage situations where non-treatment-related factors contribute to a studied toxicity. The thesis also discusses how fractionation effects as described by the linear-quadratic model may affect the modelling procedure and the modelling results. The clinical applications involve two datasets with non-small-cell lung cancer (NSCLC) patients (n=26) or localized prostate cancer patients (n=874). Patients were consecutively treated at the Sahlgrenska University Hospital in Göteborg, Sweden, 1998-2005 and 1993-2006, respectively.

The first paper presents NTCP modelling results for radiation-induced rib fractures after hypofractionated SBRT for NSCLC. The results indicate that the high-dose region is more strongly associated with rib fracture than a low dose in a large volume.

The second paper presents a survey of 21 patient-reported genitourinary symptoms among prostate cancer survivors. The toxicity profile for survivors treated with the combination of conventionally fractionated external beam radiation therapy (EBRT) and hypofractionated brachytherapy (EBRT+BT) is similar to the toxicity profile for survivors treated with conventionally fractionated EBRT.

The third paper investigates urethral pain among prostate cancer survivors and finds that higher fractionation-corrected urethral dose corresponds to higher prevalence; no such relationship is seen for absorbed dose. Survivors with three years to follow-up report urethral pain more frequently than survivors with more than three years to follow-up.

The fourth paper suggests a method to estimate composite doses in pelvic OARs after prostate cancer EBRT+BT with limited treatment information. It was motivated by the lack of BT dose information in the prostate cancer dataset. The method produces robust estimations for OARs located far from the prostate, but estimations for OARs located close to the prostate may be less robust.

The fifth paper presents a relationship between mean urinary bladder dose (with or without fractionation correction) and urinary leakage for men treated with EBRT. Analyses are performed for survivors treated with EBRT and EBRT+BT separately as well as for the whole study population. Symptom background rates from non-irradiated controls were considered. Estimated composite urinary bladder doses by the method suggested in Paper IV are used for the EBRT+BT group.

Keywords: hypofractionation, normal tissue complication probability, modelling, linear-quadratic model, fractionation sensitivity, late toxicity, radiation-induced rib fracture, genitourinary toxicity, stereotactic body radiation therapy, high-dose-rate brachytherapy, multimodality radiation therapy, patient-reported outcomes, prostate cancer, NSCLC.

ISBN: 978-91-628-8647-9
E-publication: http://hdl.handle.net/2077/32036

CONTENTS

LIST OF PAPERS

I. **N. Pettersson, J. Nyman, K.A. Johansson;**
"Radiation-induced rib fractures after hypofractionated stereotactic body radiation therapy of non-small cell lung cancer: a dose – and volume-response analysis";
Radiotherapy and Oncology 91, 360-368 (2009).

II. **C. Olsson, N. Pettersson, D. Alsadius, U Wilderäng, S.L. Tucker, K.A. Johansson, G. Steineck;**
"Patient-reported genitourinary toxicity for long-term prostate cancer survivors treated with radiation therapy";
Under revision.

III. **N. Pettersson, C. Olsson, S.L. Tucker, D. Alsadius, U. Wilderäng, K.A. Johansson, G. Steineck;**
"Urethral pain among prostate cancer survivors 1 to 14 years after radiation therapy";
International journal of radiation oncology, biology, physics 85, e29-37 (2013).

IV. **N. Pettersson, K.A. Johansson, D. Alsadius, S.L. Tucker, G. Steineck, C. Olsson;**
"A method to estimate composite doses for organs at risk in prostate cancer treated with EBRT in combination with HDR BT";
Submitted.

V. **C. Olsson*, N. Pettersson*, D. Alsadius, U. Wilderäng, S.L. Tucker, K.A. Johansson, G. Steineck;**
"Relationships between dose to the urinary bladder or the urethra and patient-reported late genitourinary toxicity after prostate cancer radiation therapy";
* Submitted. Both authors contributed equally.

PRELIMINARY RESULTS

N. Pettersson, J. Nyman, K.A. Johansson.
"DVH analysis of radiation-induced rib fractures after hypofractionated SBRT for NSCLC".
3rd Acta Oncologica Symposium on Stereotactic Body Radiotherapy, Copenhagen 2006. (Oral presentation)

N. Pettersson, J. Nyman, K.A. Johansson.
"DVH analysis of radiation-induced rib fractures after hypofractionated stereotactic boby radiation therapy (SBRT) for non-small cell lung cancer"
Radiotherapy and Oncology, 2007, 84(S1): S68. 9th Biennial Estro meeting, Barcelona 2007. (Oral presentation)

N. Pettersson, G. Steineck, B. Lennernäs, E. Holmberg, K.A. Johansson.
"Dose-volume response analysis for urinary urgency: external beam radiotherapy alone versus external beam radiotherapy in combination with hypofractionated brachytherapy"
Radiotherapy and Oncology, 2008, 88(S2): S461. Estro27, Göteborg, 2008. (Poster)

LIST OF ABBREVIATIONS

3D	*three-dimensional*
AIC	*Akaike Information Criterion*
AUC	*area under the curve*
AVM	*arteriovenous malformation*
BMI	*body mass index*
BT	*brachytherapy*
CI	*confidence interval*
CRT	*conformal radiation therapy*
CT	*computed tomography*
CTCAE	*Common Terminology Criteria for Adverse Events*
CTV	*clinical target volume*
D_v	*maximum dose in the volume excluding (absolute or relative) volume v*
DVH	*dose-volume histogram*
EBRT	*external beam radiation therapy*
$EQDX_{\alpha/\beta}$	*equieffective dose in X-Gy fractions using α/β*
FSU	*functional subunit*
gEUD	*generalized equivalent uniform dose*
GTV	*gross tumour volume*
Gy	*Gray*
HDR	*high-dose-rate*
ICRU	*International Commission of Radiation Units and Measurements*
IMRT	*intensity-modulated radiation therapy*
LENT-SOMA	*Late Effects Normal Tissue Subjective Objective Management Analytical*
LKB	*Lyman-Kutcher-Burman*

LL	*log-likelihood*
LQ	*linear-quadratic*
LQ-L	*linear-quadratic-linear*
ML	*maximum likelihood*
MLC	*multi-leaf collimator*
MLE	*maximum likelihood estimation*
MRI	*magnetic resonance imaging*
NSCLC	*non-small-cell lung cancer*
NTCP	*normal tissue complication probability*
OAR	*organ at risk*
OTT	*overall treatment time*
POSTOP	*post-operative*
PRO	*patient-reported outcome*
PSA	*prostate-specific antigen*
PTV	*planning target volume*
QUANTEC	*quantification of normal tissue effects in the clinic*
ROC	*receiver operating characteristics*
RTOG/ EORTC	*Therapy Oncology Group in North America and the European Organization for Research and Treatment of Cancer*
SEM	*standard error of the mean*
SBRT	*stereotactic body radiation therapy*
SD	*standard deviation*
SF	*surviving fraction*
SRT	*stereotactic radiation therapy*
TPS	*treatment planning system*
$\mathbf{V_D}$	*volume receiving at least absorbed dose D*

1. INTRODUCTION

1.1 Background

Today, more than 6 million individuals worldwide receive radiation therapy as part of their cancer treatment each year [1, 2]. The ideal radiation therapy is one where there is a sufficiently high dose to eradicate the tumour and no dose at all elsewhere to avoid unwanted effects in healthy tissue. This is however not a practically achievable dose distribution, and our everyday clinical task is to arrive at the best compromise where each patient's treatment plan has a high probability of eliminating the tumour while simultaneously having a low risk of damaging the surrounding non-malignant tissues. The field of radiation therapy has the previous decades undergone considerable technological developments in patient imaging, treatment planning and delivery and we now have better means to create and deliver suitable dose distributions.

The process of treatment planning consists of three major parts. First, the patient is imaged using one or more three-dimensional (3D) imaging techniques such as computed tomography (CT), magnetic resonance imaging (MRI) or ultrasound imaging. Second, on these images, the volumes suspected to contain microscopic and macroscopic tumour tissues, and the organs we do not want to irradiate (organs at risk, OARs) are identified. In the third step, the treatment plan is created by optimizing how the dose will be distributed within the patient, i.e. how much dose that should be received by the tumour and how much the dose to the healthy organs should be restricted. The results of the treatment planning procedure are a 3D dose distribution, the absorbed dose calculated in a large number of volume elements (voxels) inside the patient,and the corresponding treatment machine settings required to deliver this dose distribution in the patient. Absorbed dose is, however, a physical quantity that describes the amount of energy from ionizing radiation absorbed per unit mass and is seldom linearly related to the biological effect in human tissue. Thus, for each treatment regimen we must not only optimize the dose distribution, but also how much dose that should be delivered at each treatment (fraction) to achieve the desired outcome. This optimization is a compromise between our competing objectives of tumour elimination and unwanted effects in normal tissue.

To deliver the planned dose to the tumour and surrounding tissue at each fraction, the patient needs to be immobilized in an accurate and reproducible position relative to the treatment machine. Current developments of patient positioning techniques involve X-ray imaging and adjustment immediately prior to treatment; this increases the correspondence between the planned and delivered absorbed dose distributions in both the tumour and surrounding OARs [3].

1.2 Fractionation

Early in the 20th century it was recognized that delivering the same amount of ionizing radiation in a large number of fractions during a longer period of time resulted in reduced normal tissue effects [4]. However, for many decades there were conflicting interpretations regarding if this was due to a time effect, a dose per fraction effect or a combination of both [4]. The relationship between overall treatment time (OTT), total dose, and dose per fraction was not understood until the late 1970's and early 1980's [5-7]. The response to altered fractionation for both normal and tumour tissue was then mathematically described by the linear-quadratic (LQ) model [5, 8]. This model was derived from the concept of cell-survival curves: the proportion of cells surviving irradiation is described with two parameters, α and β. The quotient, α/β, is the quantification of the tissue's fractionation sensitivity and if this quotient is known one can calculate the effect of a change in dose per fraction. Delivering the same total dose in a large number of fractions results in reduced normal tissue toxicity. However, the daily fraction dose cannot be arbitrarily small since this will lead to a very long OTT which in turn becomes a problem due to accelerated tumour repopulation [9, 10]. The model has also been used to design many clinical studies [11].

The LQ model was further developed to recognize other factors such as OTT, dose rate, low-dose hypersensitivity, and incomplete repair between fractions [12]. It is the model most widely utilized in the clinic today and, given knowledge on the relevant parameters, it can be expected to give results in line with observed clinical data when the dose per fraction is between 1 and 6-8 Gy. Until now, most treatments have been delivered using around 2 Gy per fraction, and the knowledge about how tumour and normal tissues respond to high doses per fraction is limited. There is currently a debate on whether the LQ model accurately describes the fractionation effect at large doses per fraction and several competing models have been suggested [13-18].

1.3 Complications and normal tissue complication probability

Unwanted radiation-induced toxicity, side effect, in normal tissue has always been an inherent risk of radiation therapy. As our treatment techniques have improved over time with regards to the irradiation of normal tissue, we have gradually learned to avoid the most debilitating complications. This has given us possibility to identify and deal with toxicity that may be considered 'less severe' but could be detrimental to the patient's quality of life. In this regard, patient-reported outcomes (PROs) are becoming an important supplement to more traditional assessments and scoring of toxicity [19].

In the early 1990's, Emami and co-workers made one of the first efforts to compile available data and present them in a form suitable for implementation in everyday clinical work [20]. They suggested dose levels for 5% and 50% risk of complication for various OARs and toxicities. Specifically, they used a 'volume parameter' to quantify how sensitive the OAR was to a change in irradiated volume – the volume effect. This meant that they had a normal tissue complication probability (NTCP) model i.e. a link between an inhomogeneously irradiated OAR and the risk of complication [21, 22]. Many such NTCP

models have been proposed over the years [23-29]. Regardless of their different aspirations on being biologically founded, they are all similar in that they consider how the total dose, the dose per fraction and the amount of irradiated volume affect the risk of complication.

To fit an NTCP model to clinical data, we need to collect information from a cohort of patients. Specifically, we need data on whether the patient experienced a complication and a description of the dose distribution from the organ(s) we suspect the complication originates from. Furthermore, organs can express radiation damage in several different ways and each of those must be separately modelled. The ideal situation for NTCP modelling is to measure a specific toxicity – an atomized symptom – and to be certain from which OAR the damage originates [30]. Once the best model (and its model parameters) has been determined, it can assist in creating treatment plans with lower risks of complication.

1.4 Hypofractionation

Hypofractionation is the use of few fractions with a high dose per fraction. The tumour dose delivered at each fraction must be at least 2.5 Gy* and should be delivered in less than 20-30 minutes. There are many ways to optimize fractionation regimens and some or all fractions can be delivered with a high dose for the regimen to be considered hypofractionated. There are some obvious advantages with hypofractionation, from both the clinical and the patient's perspective. It uses less time on expensive and maybe scarce resources in the radiation therapy department, it is more convenient for the patient since there are fewer fractions, and there may sometimes be radiobiological benefits such as the short OTT leaving little time for accelerated tumour repopulation.

However, fractionation regimens with high dose per fraction have historically been associated with increased normal tissue complications [31]. This association originates from treatments during the 1940's – 1980's when some regimens were developed using incorrect models [4, 32]. In addition to the large volumes of irradiated normal tissue during that period, these regimens failed to properly take the fractionation effect for normal tissue into account. The total dose was not sufficiently decreased to compensate for the increased effect at high doses per fraction and this sometimes resulted in severe complications [33].

1.4.1 Modern hypofractionated techniques

Technological advances in radiation therapy techniques in the 1980's and 1990's brought image-based treatment planning, multi-leaf collimators (MLCS) and novel ways to make sure the patient (and the tumour) was correctly positioned on the treatment table. This enabled us to create and deliver dose distributions with a considerably decreased volume of irradiated tissue outside the tumour. The combination of highly conformal dose distributions and a better insight in fractionation sensitivity are now creating new possibilities for hypofractionated treatments. Two techniques that make use of this are stereotactic (body) radiation therapy and brachytherapy (BT).

* No universally adopted definition of hypofractionation exists, but the dose per fraction should be notably larger than the 2-Gy fractions used in conventional fractionation.

1.4.2 Stereotactic (body) radiation therapy

Stereotactic radiation therapy (SRT) is an external beam radiation therapy (EBRT) technique that is utilized to irradiate small tumours or lesions. Special equipment is used to ensure that an accurate relationship between the patient's anatomy and the coordinate system of the treatment machine can be established. The treated lesions are preferably small, the patient is carefully set-up in the dedicated system, and a multi-leaf collimator with small leaf width is usually used. The resulting dose distributions are exceptionally conformal, but the treatment set-up procedure is time-consuming. The use of fewer fractions is thus both a possibility and a practical necessity.

SRT was initially used to treat intracranial tumours and non-malignant, malfunctioning vascular bundles (arteriovenous malformations, AVMs). In the latter case the objective was to obliterate the AVM by creating a necrosis, i.e. the normal tissue 'complication' is in this case the sought treatment effect.

Stereotactic body radiation therapy (SBRT) was introduced in the 1980's. It uses similar principles as SRT, but is applied outside the cranium [34]. So far, most experience in SBRT has been gained for liver and lung tumours, but results for prostate treatment techniques are emerging as well [35]. The rationale behind hypofractionated liver and lung SBRT, besides the poor outcomes for conventional fractionation, was that both organs were considered to tolerate high doses in small volumes [36].

1.4.3 Brachytherapy

BT is the treatment of malignant disease by means of placing a radioactive source close to or inside the tumour. The primary advantage of BT is the rapid dose fall-off outside the high-dose region resulting in less volume of normal tissue being irradiated. Radioactivity was discovered in 1896, and already as early as in the first decade of the 20th century radium (^{226}Ra) was utilized in efforts to treat tumours. For a long time, manual placement of the radioactive source was performed which led to unnecessary irradiation of the hospital staff. To overcome this problem, BT treatment machines – afterloaders – were developed in the 1960's. In an afterloader, the radioactive source is welded to the end of a wire. The afterloader is connected to one or many catheters placed in or close to the tumour and the position of the wire within each catheter can then be remotely operated. This leads to radiation protection for the staff, and by placing the source at different positions within the fixed catheters for different durations, the dose distribution can also be optimized. There are many ways to deliver BT, and the time it takes to deliver a treatment varies greatly from months in permanent implantations with iodine (^{125}I) or palladium (^{103}Pd) sources to minutes in high-dose rate (HDR) BT with sources of cobalt (^{60}Co) or iridium (^{192}Ir).

Current state-of-the art BT is an image-guided and intensity-modulated treatment modality where current interests and developments mainly are focused at cervical and prostate cancer [37, 38]. The reason for using hypofractionation in BT is simple: placing catheters within a deep-seated tumour is an invasive and time-consuming procedure and maximum benefit should be gained from each session. Using BT in combination with image-guided techniques, a highly conformal tumour dose distribution taking normal tissue irradiation into account can be achieved.

1.5 Aim of the thesis

Although several hundred papers on quantification and modelling of complications after radiation therapy are published each year, knowledge about normal tissue toxicity after hypofractionated radiation therapy is limited. It is indicative that the compilations of normal tissue tolerance doses suggested by Emami *et al.* in 1991 and the follow-up effort by QUANTEC in 2008 mainly dealt with conventional fractionation [20, 39, 40]. Hypofractionated radiation therapy is today an established technique to deliver curative radiation therapy and more knowledge about how radiation-induced effects arise is essential to improve treatments for future patients.

The work described in this thesis aims to investigate normal tissue complications in hypofractionated radiation therapy through the development of methods and their application to clinical data. In particular, the objectives are:

- to derive a dose-response curve for treatments delivered with a fixed number of fractions where the fractionation effect is taken into account,
- to apply the derived dose-response curve in NTCP modelling of radiation-induced rib fractures following hypofractionated SBRT for non-small-cell lung cancer,
- to investigate relationships between urethral doses and urethral pain in conventionally and hypofractionated radiation therapy for prostate cancer,
- to develop a method to estimate composite doses in combined EBRT and BT when image and dose information for BT is lacking, and
- to use composite doses and information from a non-treated population in NTCP modelling of genitourinary toxicity after prostate cancer radiation therapy.

2. BACKGROUND

In NTCP modelling the aim is to determine a relationship between the delivered dose distribution in a volume of normal tissue and a specific toxicity that originates from that same tissue. The mathematical formulation of this relationship is called an NTCP model and included in this formula are model parameters that are specific to each combination of OAR and studied toxicity. The minimum requirements needed to establish the relationship, i.e. to determine the model parameters, are a description of the delivered dose and a systematic evaluation of the toxicity of interest in a cohort of patients. Once the model and its parameters are known, it can guide us in the treatment planning process to minimize the risk of this complication for future patients.

There are typically three tissue- and toxicity-specific OAR properties that we want to consider for a risk of radiation-induced complication: the effect of the total dose, the effect of the dose per fraction and the effect of different dose distributions within the OAR. The mathematical structure of NTCP models consider this and the determined corresponding parameter values will reflect the tissue properties. Calculating the NTCP for a given dose distribution typically consists of two steps: first, the 3D OAR dose distribution is summarized into a single representative value, and second, this representative value is used to calculate the probability of a given complication.

There are two concepts of tissue response that have been proposed and that are relevant for the feasibility of hypofractionated radiation therapy. A serial-type tissue is thought of as having subvolumes organized in a chain-like structure and damaging one small part has adverse effects on the overall function of the tissue [41]. For serial-type tissues, it is the highest dose that mainly determines the risk of complication. In contrast, the function of a parallel-type tissue is the sum of contributions from each subvolume and damaging one small part will have little effect for the overall response. For parallel-type tissues, the dose averaged over all subvolumes (the mean dose) mainly determines the risk of complications. The concepts of serial-type and parallel-type tissue are closely related to the volume effect. A tissue that is insensitive to changes in mean dose is said to have a small volume effect and vice versa. Examples of serial and parallel tissues are the spinal cord and lung, respectively.

2.1 Fractionation in radiation therapy

2.1.1 The linear-quadratic model and survival curves

The LQ is model used as a means to quantify the surviving proportion of irradiated tumour cells [41]. The change in the surviving fraction (SF) of tumour cells with dose is described by the equation

$$SF(d)=e^{-(\alpha d+\beta d^2)} \tag{2.1}$$

where α (Gy^{-1}) and β (Gy^{-2}) are parameters quantifying the radiation sensitivity, and

d is the absorbed dose. α/β describes the shoulder of the survival curve when plotted in a linear-logarithmic diagram (Figure 2.1, solid curves). When the quotient is small, cells are more sensitive to changes in the dose per fraction, i.e. they have a larger fractionation sensitivity. If the time between two irradiations is sufficiently long, it can be assumed that all repairable damage inflicted by the first irradiation has been completely repaired, and a new cell survival curve can be superimposed on the first. According to the LQ model, the surviving proportion of cells after n fractions (all of dose d) will be

$$SF(D)=[e^{-(\alpha d+\beta d^2)}]^n=e^{-(\alpha nd+\beta nd^2)}=e^{-(\alpha D+\beta dD)} \quad (2.2)$$

where the total absorbed dose D is given with n fractions, each of absorbed dose d (Figure 2.1, dashed curves) [41].

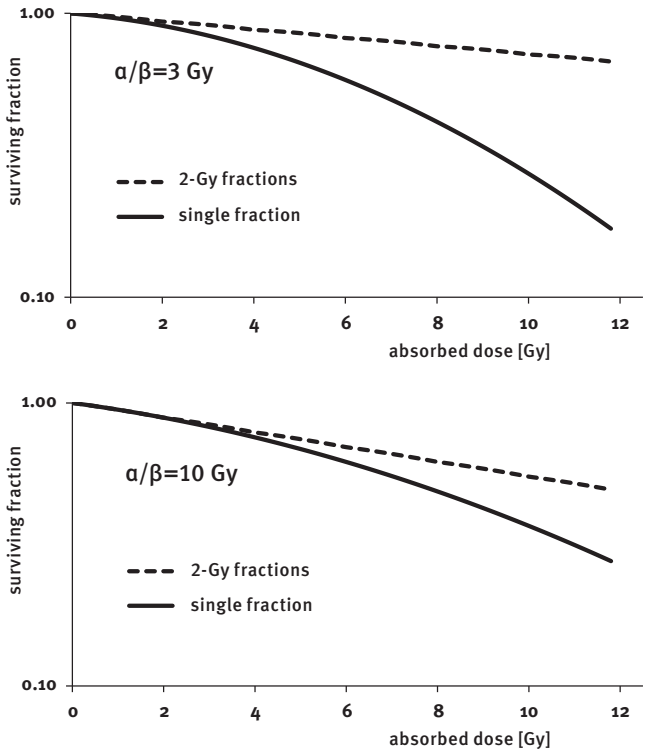

FIGURE 2.1. Survival curves for two different α/β delivered in a single fraction (solid curves) or in 2-Gy fractions (dashed curves). Top: α/β=3 Gy, bottom: α/β=10 Gy.

2.1.2 Isoeffect calculations

Calculating the "effect" E from a fractionated treatment is typically done using the negative logarithm of Eq. (2.2)

$$E=\alpha D+\beta dD=D(\alpha+\beta d), \quad (2.3)$$

which can be generalized to n fractions of arbitrary dose d_i

$$E=\sum_{i=1}^{n} \alpha d_i+\beta d_i^2 \ . \tag{2.4}$$

Furthermore, to get a clinically familiar reference from conventional fractionation for this "effect", it is converted into what usually is denoted the equivalent dose in 2-Gy fractions (EQD_2) or the biological equivalent dose (BED). This thesis will however follow the upcoming recommendation of the International Commission of Radiation Units and Measurements (ICRU) and use the terminology equieffective dose† [42]. If a treatment regimen is compared to another one delivered with X Gy per fraction, the equieffective dose is denoted $EQDX_{\alpha/\beta}$ where the subscript refers to the α/β value that the dose is equieffective to. The $EQDX_{\alpha/\beta}$ for several fractions is calculated

$$EQDX_{\alpha/\beta}(\alpha+\beta X)=D(\alpha+\beta d) \tag{2.5}$$

or, in the general case,

$$EQDX_{\alpha/\beta}=D\,\frac{(d+\alpha/\beta)}{(X+\alpha/\beta)}=\frac{\sum_i d_i(d_i+\alpha/\beta)}{(X+\alpha/\beta)}. \tag{2.6}$$

The EQD2 and BED become special cases of $EQDX_{\alpha/\beta}$ denoted $EQD2_{\alpha/\beta}$ and $EQDO_{\alpha/\beta}$, respectively. The role of α/β as a measure of the fractionation sensitivity is evident: a low (high) α/β value, results in large (small) changes in $EQDX_{\alpha/\beta}$.

Extensions to the LQ model to include the incomplete repair between fractions, the dose-rate effect, and corrections for OTT have been suggested [12]. Neither of these extensions were considered necessary for the included papers and will therefore not be further discussed in this thesis.

2.1.3 The linear-quadratic model for normal tissue

The LQ model was introduced as a means to describe the SF of tumour cells after irradiation, but it is widely applied to normal tissues as well [41]. While its biological interpretation is straightforward for tumours, where we aim to eradicate tumour cells, it is less clear what the target cells for normal tissue may be. The concept of functional subunits (FSUs) has been proposed together with the concepts of serial and parallel tissue organization [29]. But for a specific organ it is not clear which structure within the organ this FSU corresponds to. Although a radiobiological interpretation of the LQ model for normal tissue may be beneficial or interesting, it is not necessary for NTCP modelling. For this purpose, it is enough to recognize that it is a model that provides fits in good correspondence with observed data. However, extrapolating models to situations very

† The notations in Papers I and III and in this framework will therefore not be consistent.

different from the ones where they were established should always be done with caution.

Generally speaking, tumours have higher α/β values than normal tissue. Consequently, fractionated irradiation with small doses per fraction usually allows for a higher tumour dose and spares the surrounding tissues. On the other hand, if the tumour α/β value is equal to or lower than that of normal tissue, larger doses per fraction may be safely delivered. In cases where we do not know the actual values, generic values of 10 Gy and of 3 Gy are typically used for tumour and normal tissue, respectively [42].

2.1.4 Fractionation effects at (very) high doses per fraction

Several models have been suggested to take the effect at higher dose per fraction into account [13, 14, 16], among those is the linear-quadratic-linear (LQ-L) model suggested by Astrahan *et al.* [14]. In their model, the fractionation effect is described by the LQ model up to a dose per fraction d_t, and it then becomes linear for doses higher than d_t continuing with the same slope as at d_t. The LQ and the LQ-L models are illustrated in Figure 2.2.

$$EQDX_{\alpha/\beta}(d) = \begin{cases} d\dfrac{(d+\alpha/\beta)}{(X+\alpha/\beta)}, & d \le d_t \\ d_t\dfrac{(d_t+\alpha/\beta)}{(X+\alpha/\beta)} + (d-d_t)\left(\dfrac{2d_t+\alpha/\beta}{X+\alpha/\beta}\right), & d > d_t \end{cases} \tag{2.7}$$

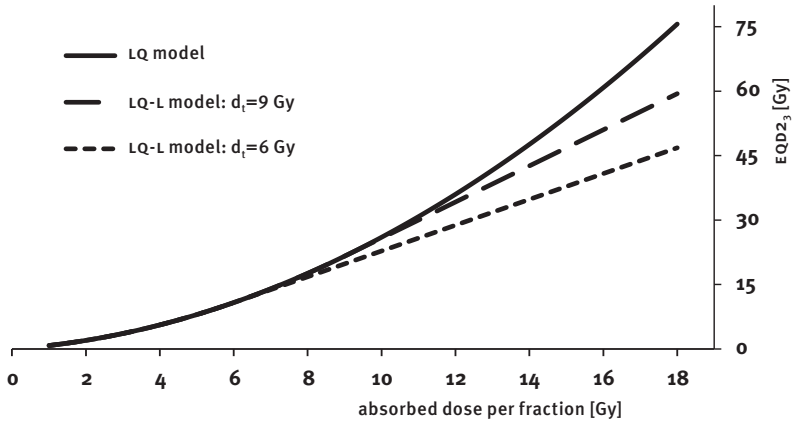

FIGURE 2.2. The LQ model and the LQ-L model for α/β=3 Gy and two different d_t.

2.2 Late toxicity following radiation therapy

Normal tissue toxicity is caused by incidental irradiation of tissue surrounding the tumour. Toxicity manifesting more than three months after completed radiation therapy is classified as late toxicity. Whether a patient experience a toxicity, or side effect, can be detected in different ways: it can be reported by a healthcare professional during follow-up, or by the patient herself or himself [41]. Specific separate efforts, prospectively or retrospectively, may also be undertaken to systematically evaluate the presence of such damage. One such example is questionnaire-collected data.

In NTCP modelling, we aim to quantify the relationship between the delivered dose in an OAR and a specific toxicity - an atomized symptom - that is "*likely to reflect specific radiation pathophysiologies*" originating from the OAR in question [19, 43]. The studied side effect should be systematically evaluated meaning that the sensitivity and specificity for its detection should ideally be the same for all subjects. Several grading systems such as the Common Terminology Criteria for Adverse Events (CTCAE, [44]), the Radiation Therapy Oncology Group in North America and the European Organization for Research and Treatment of Cancer (RTOG/EORTC, [45]), and Late Effects Normal Tissue Subjective Objective Management Analytical (LENT-SOMA, [46]) have been developed to allow for structured and consistent classification of late toxicity. Both CTCAE and RTOG/EORTC can combine different late toxicities into one grade. The LENT-SOMA system clearly separates different aspects of toxicity associated with the same OAR and also how these are scored.

A toxicity reflecting a specific underlying pathophysiology in an OAR can be measured in different ways. For instance, pain may either be assessed as 'how much' or 'how often'. Regardless if the toxicity is measured on a continuous, discrete, or categorical scale, a criterion, a cut-off, has to be set to define the complication; a task that may be difficult in itself [19]. According to this criterion, subjects will be dichotomized into either having or not having the studied side effect. Some toxicities, such as rib fracture, are naturally binary, while others, such as amount of pain, are not. The combination of toxicity and decided cut-off is denoted endpoint.

The studied endpoint in Paper I was radiation-induced rib fracture as verified by CT scan; this endpoint is binary and was scored as 1 in case of fracture and 0 if there was no fracture. In Papers II, III, and V, a wide spectrum of genitourinary toxicities after prostate cancer radiation therapy was studied. These data were taken from a postal-based questionnaire. None of these symptoms were binary and for each studied symptom cut-offs had to determined. The development of the questionnaire is described below.

2.2.1 Questionnaire development and principles

David Alsadius *et al.* developed a study-specific questionnaire according to the principles at The Divisions of Clinical Cancer Epidemiology at the Sahlgrenska Academy and the Karolinska Institute to assess the occurrence of late toxicity after prostate cancer radiation therapy [47-50]. They began with a structural assessment of previous questionnaires from the divisions concerning symptoms after pelvic irradiation or prostatectomy. They classified the questions in these questionnaires according to the symptom they measured (e.g. urinary leakage) to conceptualize clear-cut definitions of each symptom. These definitions were then operationalized into questions in the new ques-

tionnaire. To make sure that no common symptom was missing, they interviewed four prostate cancer survivors. They validated the questionnaire using 15 men (10 prostate cancer survivors) to make sure that the questions were not misinterpreted and directly understood. The questionnaire also contained questions on demographics and comorbidities.

Toxicity data collected like this are well suited for NTCP modelling. When we evaluate a symptom which may be caused by other factors besides ionizing radiation, the information from a control population may assist in determining each factors relative contribution to the studied symptom [47].

2.3 NTCP modelling

2.3.1 Dose distributions

2.3.1.1 DOSE-VOLUME HISTOGRAMS

A dose-volume histogram (DVH) is a summary of a 3D dose distribution where the spatial dose information is discarded to provide a condensed and understandable description. It will therefore not be possible to recreate the 3D dose distribution from a DVH since the spatial dose distribution is lost. In the clinical workflow, OAR DVHs are used for treatment plan comparison and to create dose distributions for inverse treatment planning. In NTCP modelling, the DVH is the most commonly used description of the OAR dose distribution to relate the delivered OAR dose to the studied toxicity.

The two most common DVH representations are the cumulative DVH and the differential DVH; if one representation is known, the other can be calculated. For treatment plan comparison, cumulative DVHs are most commonly used. The relationship between dose distribution and different DVH representations is shown below (Figure 2.3). The volume represention of a DVH is either on absolute or relative form.

A DVH can be exported as a text file from the TPS where the dose bin size is user selectable. All DVHs used for the analyses in this thesis used a dose bin size, denoted ΔD, of 0.5 Gy. An important property of the differential DVH is that the area under the curve is the volume of the OAR.

$$V = \sum_i v_i \, \Delta D \tag{2.8}$$

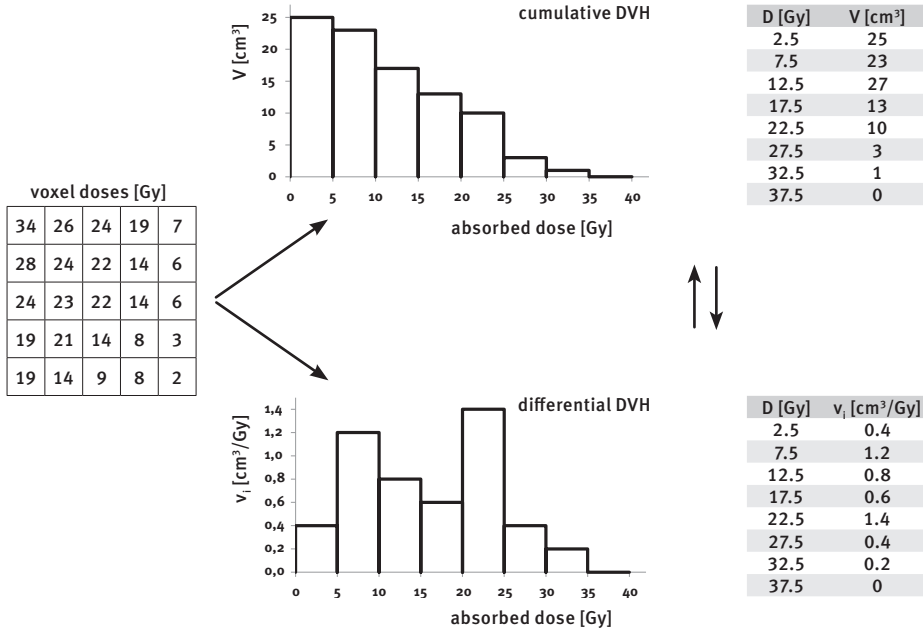

FIGURE 2.3. Relationship between dose distribution, DVHs and their tabular representation.
Left: dose distribution; absorbed dose in each 1 cm^3 volume .
Top: corresponding cumulative DVH with dose bin size of 5 Gy.
Bottom: corresponding differential DVH with dose bin size of 5 Gy.

Since the spatial dose distribution is lost, a DVH representation may have some drawbacks. If one part of the OAR is more important for organ functionality than another or if the radiation sensitivity varies over the volume, some relevant information may be lost. For oblong organs (spinal cord, rectum etc.) high doses across the OAR may cause more damage than the same dose along it.

2.3.1.2 DOSE-DISTRIBUTION DESCRIPTORS

The dose distribution in an OAR is often inhomogeneous. There are several ways to summarize a dose distribution or the DVH into one representative value, a descriptor value. The mean dose is a common measure of the total dose in a volume. It is routinely reported by the TPS and it can also be calculated from any of the DVH representations.

The cut-off volume (D_V) and cut-off dose (V_D) descriptors are other common ways to summarize a DVH into one value [27]. Despite their names, cut-off dose defines a volume and vice versa. V_D denotes the volume receiving at least dose D, and D_V denotes the minimum dose in the volume v receiving the highest dose. Their relationships to a cumulative DVH are shown in Figure 2.4. Since a cumulative DVH use either relative or absolute volume, these dose descriptors do so too.

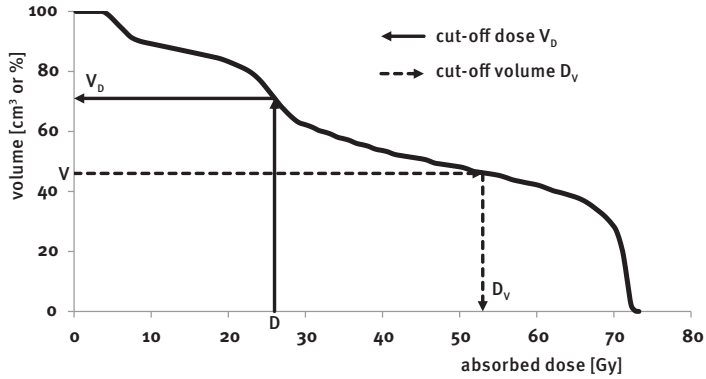

FIGURE 2.4. Visual depiction of cut-off volume and cut-off dose. The cumulative DVH can be on either absolute or relative volume form and this will affect the cut-off parameters accordingly.

The simplest description of the maximum dose is by the highest voxel dose. However, this maximum dose may not be placed at the same OAR location for each fraction, and considering that the volume of each voxel typically is a few mm^3, this measure may not be biologically relevant. The ICRU denotes the near-maximum dose as the $D_{2\%}$ [51]. In an analogues definition, the ICRU report no. 58 recommend that D_{2cm^3} should be reported for interstitial BT [52]. Both $D_{2\%}$ and D_{2cm^3} are considered in Papers IV and V. The D_{2cm^3} has the advantage that the entire OAR may not need to be contoured or encompassed by the field-of-view during image acquisition. The difference between maximum dose and near-maximum dose can be large for dose distributions delivered with steep dose gradients.

Cut-off descriptors have been used in NTCP modelling [27]. However, they only consider a limited aspect of the DVH; two DVHs with very different shapes may still have some D_V and V_D in common. Different ways to take the entire shape of the DVH into account have been proposed [53-55]. One example is D_{eff} which is calculated for a differential DVH as

$$D_{eff} = \left[\frac{\Delta D}{V} \sum_i v_i D_i^{1/n} \right]^n \tag{2.9}$$

where n is the volume effect parameter [21, 22, 54]. When n=1 the result is the mean dose and when $n \to 0$ D_{eff} becomes the maximum dose. When D_{eff} is used together with the probit dose-response curve, Eq. (2.12a), it is called the LKB model. The D_{eff} is equivalent to the (later suggested) generalized equivalent uniform dose (GEUD), where the parameter a=1/n is used instead [55].

2.3.2 Overview of dose-response curves

The relationship between dose and the risk of a given toxicity is usually modelled by an s-shaped function – also referred to as a dose-response or an NTCP curve. The curve is usually characterized by its position (D_{50}) and steepness (γ_{50}) (Fig 2.5) [56-58]. D_{50} is the dose required for a 50% risk of complication and γ_{50} is the normalised dose-response

gradient or the steepness (Figure 2.5). γ_x is generally defined as

$$\gamma_x = D_x NTCP'(D_x) \tag{2.10}$$

for an arbitrary response level x. γ_{50} has the suitable interpretation that an increase in 1% at D_{50}, increases the NTCP by γ_{50} percentage points. There are many mathematical options to describe dose-response curves, but regardless of which specific formula is used, the curves are in many cases completely described by D_{50} and γ_{50}.

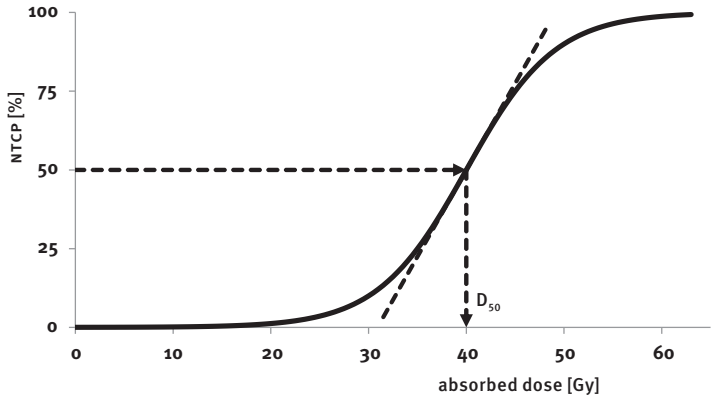

FIGURE 2.5. Position (D_{50}) and slope at D_{50} of a dose-response curve. The relation between the slope and the steepness is given by Eq. (2.10).

Various expressions such as the logistic function (Eq. 2.11), the cumulative normal distribution (probit function) (Eq. 2.12a), and the log-logistic function (Eq. 2.13) are used [57]. The actual difference between them is very small (Figure 2.6) and which function to use in NTCP modelling is not critical. It can be noted that although some toxicity is so severe that we would not allow its risk be anywhere close to 50%, D_{50} and γ_{50} are still useful to describe the position and the steepness of the dose-response curve.

$$NTCP(D) = \frac{1}{1 + e^{4\gamma_{50}\left(1-\frac{D}{D_{50}}\right)}} \tag{2.11}$$

$$NTCP(u) = \frac{1}{\sqrt{2\pi}} \int_{-\infty}^{u} e^{-\frac{t^2}{2}} dt \tag{2.12a}$$

$$u(D) = -\sqrt{2\pi}\gamma_{50}\left(1-\frac{D}{D_{50}}\right) \tag{2.12b}$$

$$NTCP(D) = \frac{1}{1+\left(\frac{D_{50}}{D}\right)^{4\gamma_{50}}} \tag{2.13}$$

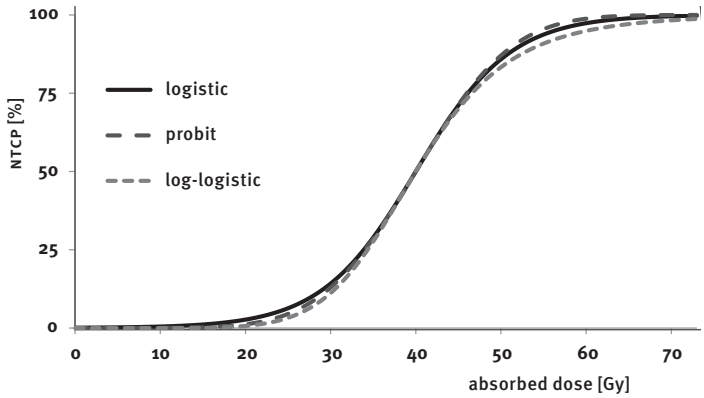

FIGURE 2.6. Logistic, probit and log-logistic dose-response curves.

2.3.3 Consideration of fractionation effects in NTCP modelling

As stated in the beginning of this chapter, calculating the NTCP typically involves two steps: first, calculating one value that will represent the entire dose distribution, and second, using this value as input in a dose-response curve. Consequently, the fractionation effect in NTCP modelling can be considered either in the first or in the second step; how this can be done is outlined in sections 2.3.3.1 and 2.3.3.2, respectively. It should also be noted that fractionation effects will be more or less present in all‡ inhomogeneous OAR dose distributions meaning that one at least needs to consider how fractionation effects will impact NTCP modelling. Some typical situations are described below:

- A fractionation correction needs to be considered when the representative value (for instance D_{eff}) takes the entire shape of DVH into account. This means that the fractionation correction occurs in the first step. An α/β value has to be selected; this may influence the modelling results.
- A fractionation correction needs to be considered when the treatment fraction size varies between fractions. This also means that the correction is done in the first step and that an α/β has to be selected; this may influence the modelling results.
- When a homogeneous dose is delivered with a fixed dose per fraction for all patients, but in a varying number of fractions, the fractionation effect is constant and will not affect the modelling results.
- If the dose is delivered with a fixed number of fractions for all patients, but with varying dose there will be different doses per fraction between patients. A dose-response curve adapted to this situation was derived in Paper I. α/β is explicitly included in that expression, but as shown below in section 2.3.3.2, the selected value will not affect the modelling results.

‡ The exception is a treatment that partially irradiates an OAR with a homogeneous dose while the rest of the OAR receives zero dose.

There is also the situation where the purpose of modelling is to estimate the fractionation sensitivity. This was briefly evaluated in Paper III for urethral pain and was also recently reported by Borst *et al.* for radiation pneumonitis following hypofractionated SBRT [59].

2.3.3.1 FRACTIONATION-CORRECTED DOSE DISTRIBUTIONS AND DVHS

This section describes representative values can be calculated from the dose distribution or the DVH with consideration of the fractionation effect. The most general approach is to perform the fractionation correction on the voxel doses in the 3D dose distribution before exporting the DVH. This is however dependent on functionality of the treatment planning system (TPS) or on independently developed software using data exported from the TPS and may consequently not always be possible.

When the entire treatment is delivered with the same OAR dose distribution, there is a more convenient way to take the fractionation effect into account. In this case, the fractionation correction can easily be performed directly on the dose column of a (cumulative or differential) DVH (see Figure 2.3). The effect is shown in Figure 2.7.

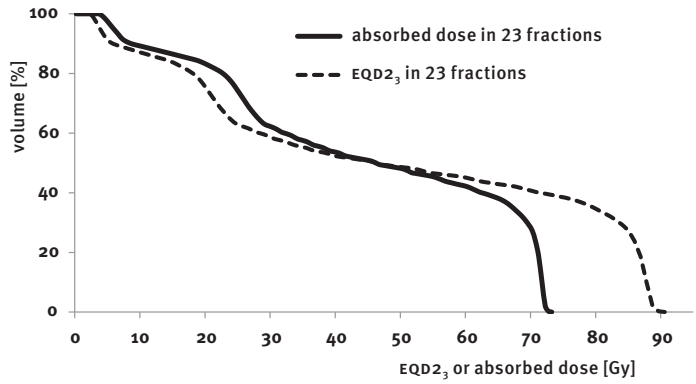

FIGURE 2.7. Cumulative DVH without and with fractionation correction assuming α/β=3 Gy and 23 fractions.

Any of the dose-distribution descriptors from the 2.3.1.2 can then be calculated in fractionated-corrected versions. Specifically, the fractionation-corrected effective dose, $EQD_{eff}X_{\alpha/\beta}$ is calculated as

$$EQD_{eff}X_{\alpha/\beta}=\left[\frac{\Delta D}{V}\sum_i v_i\left(\frac{D_i(d_i+\alpha/\beta)}{(X+\alpha/\beta)}\right)^{1/n}\right]^n. \quad (2.14)$$

Correcting for fractionation effects can be more challenging if the treatment is delivered with different dose distributions, as for instance in multiple-phased or multimodality treatments [60]. Even if we can create a treatment plan sum in the TPS, this is usually the sum of the absorbed dose distributions i.e. the fractionation effect is ignored. The general solution is to apply the fractionation correction for the contributing 3D dose

distributions before they are added. This depends, as mentioned above, on the functionality of the TPS. Exporting and using one DVH for each contributing dose distribution does not work in the general case since the spatial dose information is lost when the DVH is calculated and the risk is to add doses from different voxels.

2.3.3.2 FRACTIONATION-CORRECTED DOSE-RESPONSE CURVES

This section describes how dose-response curves can be used to take the fractionation effect into account. Again α/β from the LQ model is used to describe the fractionation sensitivity, but the following can be adapted to any model.

In Paper I, we stated that there are two different types of dose-response curves. This was however not entirely true as there actually are three types.

- In the first case we have the same fractionation effect for all patients. The same dose d per fraction is delivered in a different number of fractions for different patients.

$$NTCP(D) = \frac{1}{1+e^{4\gamma_{50,d}\left(1-\frac{D}{D_{50}}\right)}} \quad \textbf{(2.15)}$$

  The fractionation sensitivity is implicitly included in this expression since the value of D_{50} is dependent on the dose per fraction d. A subscript d is added to define a $\gamma_{50,d}$ that denotes the steepness for a situation where the dose per fraction is constant. It can be shown that $\gamma_{50,d}$ is independent of the dose per fraction d [57, 58].

- In the second case there is a different dose per fraction between patients, but the same number of fractions is delivered for all patients, that is, we have different fractionation effects between patients. This dose-response curve is derived in Paper I using the LQ model.

$$NTCP(D) = \frac{1}{1+e^{4\gamma_{50,n}\left[\frac{\frac{D_{50,n}}{n}+\frac{\alpha}{\beta}}{\frac{2D_{50,n}}{n}+\frac{\alpha}{\beta}}\right]\times\left[1-\frac{D}{D_{50}\left(\frac{D_{50}}{n}+\frac{\alpha}{\beta}\right)}\left(\frac{D}{n}+\frac{\alpha}{\beta}\right)\right]}} \quad \textbf{(2.16)}$$

  The fractionation sensitivity is explicitly included in this expression. A subscript n is added to define a $\gamma_{50,n}$ that denotes the steepness for a situation where the number of fractions is constant. α/β has to be included, but it can be shown that its value will be less important (see later in this section). This expression is applied to radiation-induced rib fractures in Paper I.

- The third case is the general situation. Now both the dose per fraction and the number of fractions are allowed to vary.

$$NTCP\left(EQDX_{\alpha/\beta}\right) = \frac{1}{1+e^{4\gamma_{50,d}\left[1-\frac{EQDX_{\alpha/\beta}}{EQD_{50}X_{\alpha/\beta}}\right]}} \tag{2.17}$$

  In this case we must also explicitly take the fractionation sensitivity into account, but this is done prior to using this expression. The steepness for this curve is the same as in Eq. (2.15).

From the expression for the equieffective dose in Eq. (2.6) it becomes clear that Eq. (2.15 and 2.16) are special cases of the general expression in Eq. (2.17). Furthermore, the relationship between the steepness for a treatment delivered with fixed dose per fraction ($\gamma_{50,d}$) and one delivered with a fixed number of fractions ($\gamma_{50,n}$) was also derived in Paper I; a result previously obtained by Bentzen [56]:

$$\gamma_{50,d} = \gamma_{50,n}\left[\frac{\frac{D_{50}}{n}+\alpha/\beta}{\frac{2D_{50}}{n}+\alpha/\beta}\right] . \tag{2.18}$$

Both $\gamma_{50,d}$ and $\gamma_{50,n}$ can be used in Eq. (2.16), but to keep the interpretation of the normalized dose-response gradients they must be used in the right context. Using Eq. (2.15) and Eq. (2.16), will give the same result if the α/β value or n are very large; in this case $\gamma_{50,d}$ and $\gamma_{50,n}$ will be equal as well.

A dose-response curve for a fixed dose per fractions is less steep than a dose-response curve for a fixed number of fractions, Figure 2.8. In the latter case, when the total dose is increased (decreased), the dose per fraction is increased (decreased) as well.

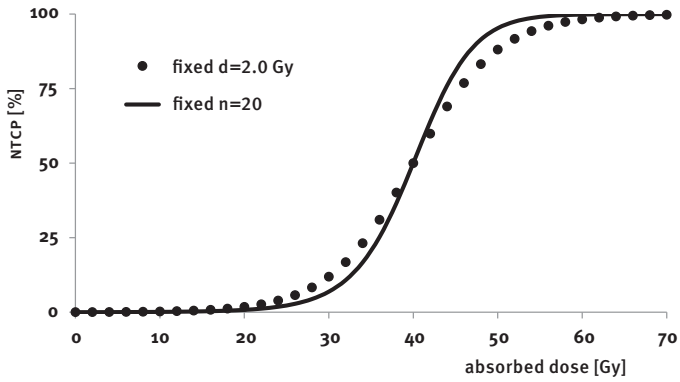

FIGURE 2.8. Dose-response curves for a fixed dose per fraction (dotted curve) and a fixed number of fractions (solid curve).

We initially thought that if the dose-response curve for a treatment delivered with a

fixed number of fractions could be accurately described using Eq. (2.16), we would be able to estimate the value of α/β. Dose-response curves plotted for different values of α/β, however, showed very little separation (Figure 2.9).

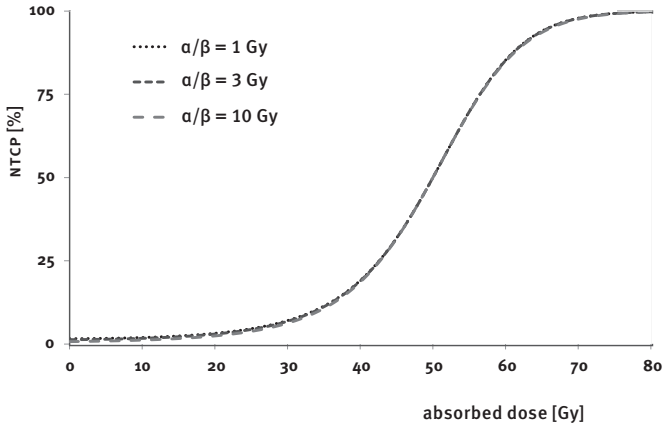

FIGURE 2.9. Dose-response curves for a three-fraction treatment using different values of α/β; D_{50}=50 Gy and $\gamma_{50,n}$=2.0 for all curves.

The potential consequences for NTCP model parameter estimation in this situation can be quantified using a simulated dataset (see section 2.4 for statistical methods). Assume that the correct model has the parameters D_{50}=50 Gy, $\gamma_{50,n}$=2.0, and α/β=3.0 Gy and that the treatment is delivered in three fractions. For this 'treatment' we have observed 11.2 % risk of complication at 35.0 Gy, 50.0% at 50.0 Gy and 85.2% at 60.0 Gy using 200 patients at each dose level. The value of the log-likelihood function, Eq. (2.21), is directly proportional to the size of the dataset, that is, the size of the simulated dataset does not impact the estimation of the best fitting parameters. Parameter estimation for Eq. (2.16) was done using values of α/β from 0 to 10 Gy, in steps of 1 Gy, and for an infinite α/β value. After substituting Eq. (2.18) into Eq. (2.16), $\gamma_{50,d,}$ was also estimated from these data. Furthermore, parameters for Eq. (2.15) were estimated as well.

The maximum value of the log-likelihood function revealed that D_{50}, $\gamma_{50,n}$ as well as $\gamma_{50,d}$ showed little dependence of α/β values from 0 to 10 Gy (Figure 2.10, panels A-D). The estimated $\gamma_{50,d}$ in panel D was related to the estimated $\gamma_{50,n}$ in panel C exactly as predicted by Eq. (2.18). Parameter estimation using Eq. (2.15) resulted in a somewhat lower D_{50}, but the maximum value of the log-likelihood function was not notably different even under these highly ideal conditions. The estimated steepness using Eq. (2.15), $\gamma_{50,d}$=1.88, was however much larger compared to the otherwise estimated $\gamma_{50,d}$ in panel D. The resulting dose-response curves and the underlying simulated dataset are shown in Figure 2.11.

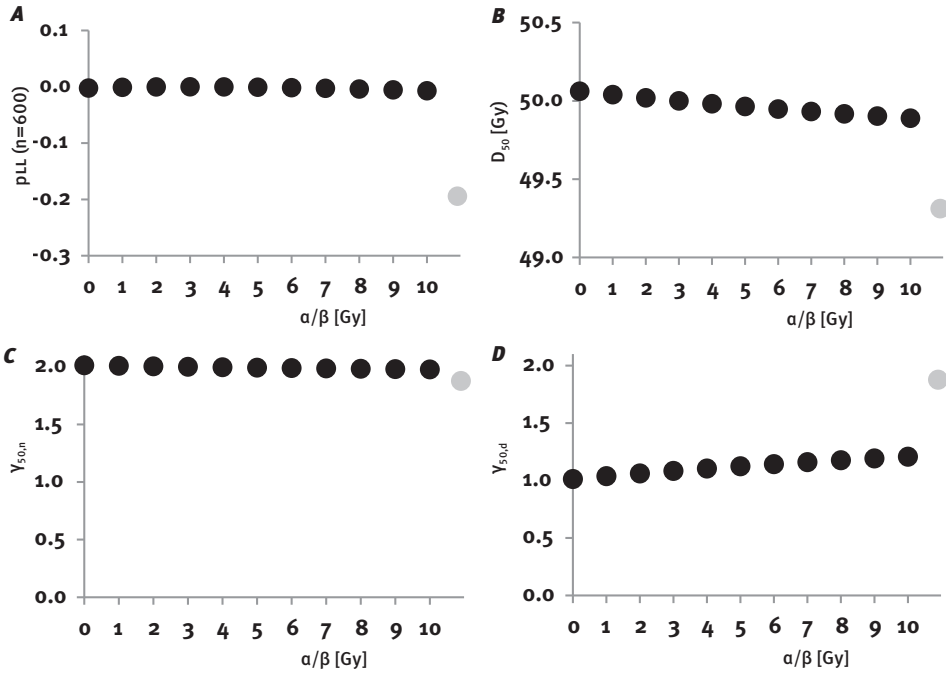

FIGURE 2.10. Analyses of the impact of different α/β values on estimated parameters using Eq. (2.16) for the simulated 600 subjects.
A: Profile log-likelihood (pLL) values; pLL for grey dot is estimated using an infinite α/β value.
B: Estimated D_{50}; D_{50} for grey dot is estimated using an infinite α/β value.
C: Estimated $\gamma_{50,n}$; $\gamma_{50,n}$ for grey dot is estimated using an infinite α/β value.
D: Estimated $\gamma_{50,d}$; $\gamma_{50,d}$ for grey dot is estimated using Eq. (2.15).

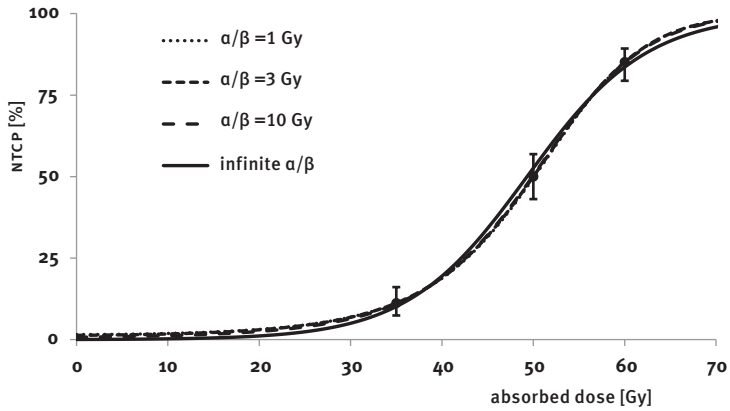

FIGURE 2.11. Estimated dose-response curves for α/β=1 Gy, α/β=3 Gy, α/β=10 Gy, and for Eq. (2.15). The vertical error bars show the 95% CI for the simulated 200 subjects per dose level.

A few conclusions can be drawn from this. Robust estimations of D_{50} and $\gamma_{50,n}$ are feasible even though we do not know the α/β value. Ignoring fractionation effects and estimating parameters using Eq. (2.15) will result in equally good model fits and reasonably

similar D_{50}, but the estimated steepness is somewhat different.

Even though using Eq. (2.15) resulted in an equally good model fit in this simulated dataset, there will be consequences when adapting the dose-response curve to other fractionation regimens. For instance, correctly calculating the dose-response curve parameters to the equieffective dose in 10-Gy factions, $EQD10_3$, will give a D_{50} and a steepness of 75.6 Gy and 1.08, respectively. However, first using Eq. (2.15) for parameter estimation and then not realizing that the steepness depends on the treatment situation will result in an incorrect dose-response curve (Figure 2.12). If we accept a maximum risk of 10% for this complication, we will set our dose limit at $EQD10_3$=52 Gy with the incorrect steepness, but the risk at this dose is actually 20% with the correct steepness.

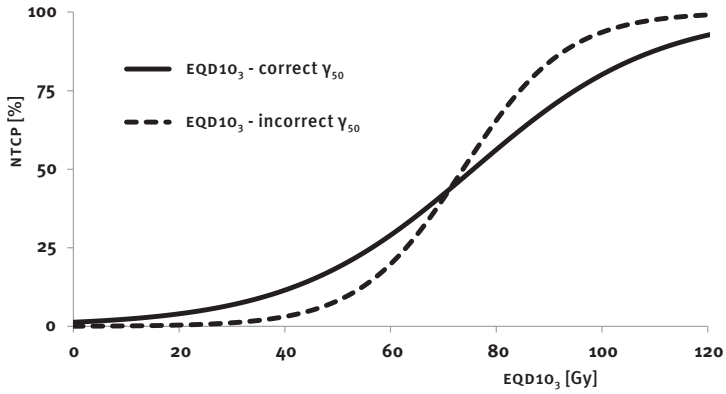

FIGURE 2.12. Dose-response curves for equieffective dose in 10-Gy fractions, $EQD10_3$, using either the correct steepness (solid curve) or the incorrect steepness (dashed curve).

The steepness of a dose-response curve for a fixed number of fractions partly originates from the fractionation effect and partly from the inherent steepness. Using Eq. (2.15) instead of Eq. (2.16) for parameter estimation when the treatment is delivered with a fixed number of fractions means that the fractionation effect is ignored and this will lead to an overestimation of the inherent steepness. To utilize an estimated dose-response curve in other fractionation regimens, the γ_{50} as well as the D_{50} must be recalculated using Eq. (2.18) and Eq. (2.6), respectively.

2.3.4 Incorporation of non-treatment-related factors in NTCP modelling

There are circumstances in where the NTCP is needs to be modelled using a dose-response curve with a restricted risk range. This may be the case when the studied endpoint is present among non-treated subjects or when the risk of the endpoint cannot be larger than a certain value. In the general case, this can be described by the following equation (exemplified by using the logistic dose-response curve with absorbed dose)

$$NTCP(D) = B + \frac{T - B}{1 + e^{\frac{4\gamma_{50}}{T-B}\left(1-\frac{D}{D_{50}}\right)}} \quad . \tag{2.19}$$

Here B denotes the risk for subjects that experience a toxicity for other reasons than irradiation and T denotes the maximum attainable risk. B may reflect the occurrence rate of a studied toxicity in a non-irradiated control population (background rate). Since B can be larger than 50%, the usual definition of D_{50} is inappropriate and D_{50} in Eq. (2.19) is interpreted as the dose required to increase the risk by half the distance between B and T and the γ_{50} is the steepness at that dose (see Figure 2.13). There are other methods to include clinical factors in NTCP modelling such as those described by Tucker *et al.* and El Naqa *et al.* but those were not explored in this thesis [61, 62].

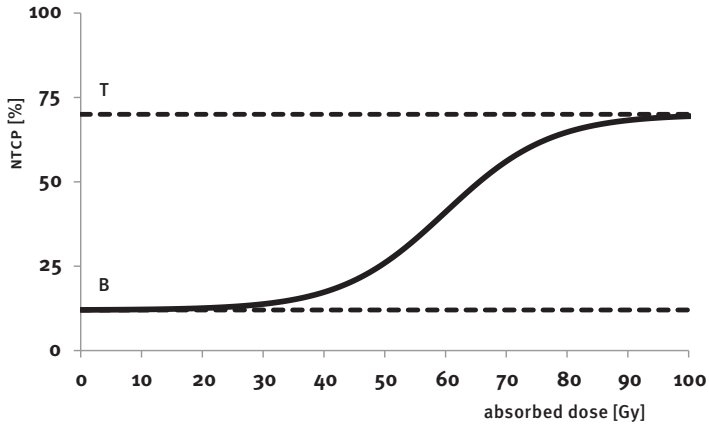

FIGURE 2.13. A dose-response curve that is restricted to values between B and T.

2.4 Statistical methods

2.4.1 Maximum likelihood estimation

Maximum likelihood estimation (MLE) is a commonly used method to estimate NTCP model parameters from a dataset with known dose distributions and binary endpoints (0 for no toxicity and 1 for toxicity). This is done by calculating the logarithm of the likelihood function, the log-likelihood (LL) function, according to [63]

$$LL(p_k \mid D_{i,j}) = \sum_{i=1}^{N} \log(NTCP_i(p_k \mid D_i)) + \sum_{j=1}^{M} \log(1 - NTCP_j(p_k \mid D_j)) \quad \textbf{(2.20)}$$

where p_k represents the k NTCP model parameters to be estimated; D_i and D_j are the known doses for N subjects with toxicity and M subjects without toxicity, respectively. The combination of parameters p_k that maximizes the value of the LL function is the parameter value combination that best describes the observed outcome for the dataset in question. The maximum value of the LL function is denoted ML and the correspond-

ing estimated parameters the maximum likelihood estimates.

Obtaining the ML by numerical optimization techniques cannot be guaranteed since the optimization procedure may converge to a local maximum of the LL function instead of finding the global maximum. This can be avoided by calculating the entire LL landscape, that is, calculating the LL function for a large number of combinations of p_k. The ML and corresponding maximum likelihood estimates can then easily be found. One need to make sure that the relevant range for each parameter is included in the calculation and that the resolution of the parameters is sufficiently high. This brute force method may be time-consuming, especially if the number of model parameters is large, but it has the advantage that the LL landscape only needs to be calculated once and the result can be saved for analyses at a later time.

2.4.2 Parameter confidence intervals and NTCP uncertainty

One-dimensional confidence intervals (CI) for the maximum likelihood estimates were calculated using the profile log-likelihood method [63]. The profile LL function for parameter p_1 among the k parameters to be estimated is given by

$$pLL(p_1)=max(LL(p_{2\text{-}k}|D_{i,j},p_1)) \tag{2.21}$$

where $p_{2\text{-}k}$ are the remaining k-1 model parameters. The CI at the significance level α for p_1 is then obtained by finding all parameter values where

$$ML-pLL(p_1)\leq 0.5\chi^2(1-\alpha,1) \tag{2.22}$$

is fulfilled. The $\chi^2(1\text{-}\alpha, 1)$ denotes the chi-square distribution with one degree of freedom for the chosen significance level α [63]. In practice both the 68% and 95% CI are calculated; these correspond to $0.5\chi^2$ values of 0.49 and 1.92, respectively. When the entire LL landscape has been calculated, the profile log-likelihood CIs are easily obtained by selecting the appropriate parameter range according to Eq. (2.22).

The uncertainty in parameter estimates will impact the estimated NTCP. This has been extensively analysed by Schilstra *et al.* [64]. Another less computationally intensive approach was suggested by Gagliardi *et al.* [65]. Assume that the ML has been estimated for the dose-response curve parameters D_{50} and γ_{50}, and that the entire LL landscape has been calculated as well. The confidence region at the significance level α of D_{50} and γ_{50} is defined as the region for which all (D_{50}, γ_{50}) combinations satisfy

$$ML-LL(D_{50},\gamma_{50})\leq 0.5\chi^2(1-\alpha,2). \tag{2.23}$$

To calculate the NTCP CI for one dose level of the dose-response curve, NTCP values are calculated for all parameter combinations within the confidence region. The CI at this dose level is now defined by the range between the minimum NTCP value and maximum NTCP value.

2.4.3 Model comparison

For comparison of different models fitted to the same dataset, the Akaike Information Criterion (AIC) can be used [63].

$$AIC = -2 \times ML + 2 \times k. \quad (2.24)$$

Here ML and k once again denotes the maximum value of the LL function and the number of parameters, respectively. Comparing models, the smaller the AIC, the better the model. The AIC provides a measure to avoid overfitting, i.e. to include parameters that do not substantially improve the fit.

2.4.4 Receiver-operating characteristics

Maximum likelihood estimation will find the best fitting NTCP model parameters and the AIC will indicate the better model among a set of competing models. It will, however, not reveal if the best model can assist in discriminating those with toxicity from those without toxicity. ROC investigates how a binary classifier discriminates responders from non-responders by setting a decision level (Figure 2.14) [66-68]. The sensitivity is the proportion of responders that were correctly categorized according to the decision level. The specificity is the corresponding proportion of non-responders that were correctly categorized.

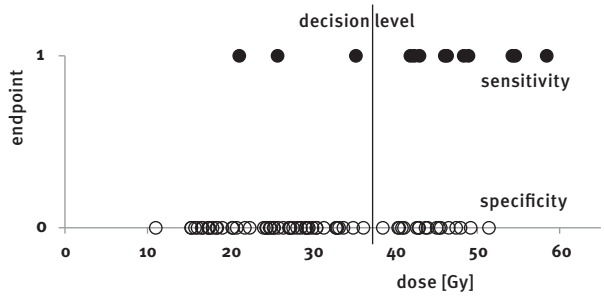

FIGURE 2.14. Principle of obtaining an ROC curve by calculating the sensitivity and the specificity at each position of the decision level.

By letting the decision level span the entire range of doses and calculate the sensitivity and specificity at each level, an ROC curve is traced (Figure 2.15).

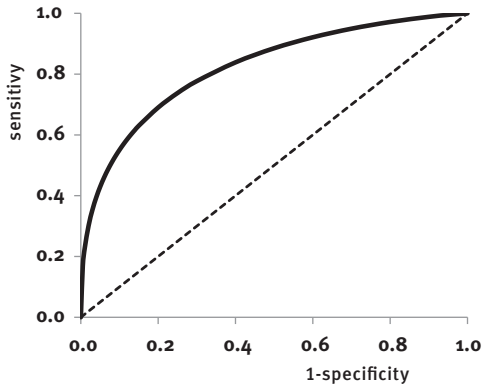

FIGURE 2.15. The ROC curve obtained from Figure 2.14.

The area under the curve (AUC) will then reveal the model's ability to discriminate responders from non-responders. In Figure 2.14, the horizontal axis is dose, but could have been the calculated NTCP; ROC evaluates the order in which responders and non-responders will appear. For a poor model, the order between responders and non-responders is random and the AUC will be the 0.5, i.e. no better than flipping a coin. If the AUC is 1, the model has created a perfect separation; this is however unattainable in radiation therapy since there always will be a dose range occupied by both responders and non-responders.

3. HYPOFRACTIONATED RADIATION THERAPY AND LATE TOXICITY

3.1 Non-small-cell lung cancer – rib fractures (Paper I)

During routine follow-up of lung cancer patients treated with hypofractionated radiation therapy at the Sahlgrenska University Hospital, a few cases of radiation-induced rib fractures were found after patients reported pain originating from the treated area. This initiated a systematic investigation among all patients and subsequently an NTCP modelling effort to analyse the risk of radiation-induced rib fracture. Mathematical expressions for dose-response curves taking the fractionation effect into account were also derived.

3.1.1 Non-small-cell lung cancer

Lung cancer is a common form of cancer in Sweden with about 3600 new cases each year [69]. It is the overall leading cause of cancer-related deaths among Swedes; 3500 died of the disease in 2010 [70]. There are two major types of lung cancer: small-cell lung carcinoma and non-small-cell lung carcinoma (NSCLC); in this thesis only patients with NSCLC are investigated.

The major cause of NSCLC is a history of smoking which represents about 85% of cases [71]. The extent of the disease at diagnosis determines treatment options and is a strong predictor of expected outcome [72]. This makes correct staging essential. For stage 1 NSCLC – localized tumour with no lymph node involvement - surgery, with or without adjuvant chemotherapy, is currently the primary treatment option with curative intent. However, some patients are medically inoperable due to comorbidity and a few refuse surgery. Hence, radiation therapy, with or without chemotherapy, has been the alternative therapeutic modality for these patients.

3.1.2 Radiation therapy

Using conventionally fractionated radiation therapy to total doses of 60-70 Gy for stage 1 NSCLC has generally resulted in poor tumour control with a typical local recurrence rate of 40% [73]. In the attempts to achieve better local control and survival, the prescribed doses have been increased over the years [74-76]. This became possible with the introduction of 3D conformal radiation therapy (CRT) keeping the volume of irradiated healthy lung low and keeping the often dose-limiting radiation-induced pneumonitis at a tolerable level. However, using conventional fractionation, the increased prescribed dose was counteracted by the increased OTT that negatively impacted tumour control [74, 76, 77]. SBRT was developed at the Karolinska University Hospital, Stockholm,

Sweden in the early 1990's for patients with liver tumours or lung metastases [34, 36]. In order to improve the poor outcome of conventional treatments and encouraged by the positive results from intracranial stereotactic treatments, they argued that

> *[t]he proposed method can be expected to give favourable results for tumours in large organs with a high tolerance to partial volume irradiation. Thus, liver and lung are organs that could be expected to be suitable for treatment of relatively large targets with this method. [36]*

To decrease the risk of treatment-related toxicity in OARs with high tolerance to partial volume irradiation, the irradiated volume outside the tumour must be kept small. This was primarily accomplished by a dedicated patient set-up device – a stereotactic body frame – that had been developed to be used together with a standard linear accelerator. The body frame enabled an accurate patient positioning relative to the linear accelerator. The body frame also included an optional diaphragm press to control tumour motion due to breathing. This set-up made it possible to have small clinical target volume (CTV) margins keeping the irradiated volume of normal tissue small. To further decrease the dose outside the planning target volume (PTV), they employed a treatment planning strategy where the dose was prescribed to the periphery of the CTV and the central part of the tumour received considerably more than 100% [36]. The first patients were treated with 1-3 fractions.

3.1.3 Stereotactic body radiation therapy at the Sahlgrenska University Hospital

The principles developed at the Karolinska University Hospital were adopted at the Sahlgrenska University Hospital for medically inoperable NSCLC patients and the first patient was treated using the stereotactic body frame (Elekta AB, Sweden; Figure 3.1) in September 1998. Encouraging treatment results for the first 45 patients were reported in 2005: 39 months median overall survival and little toxicity [78]. The treatment at the Sahlgrenska University Hospital was (and is still) prescribed to 45 Gy in three fractions and is to be delivered in less than one week. The prescribed dose is the minimum dose at the periphery of the PTV.

FIGURE 3.1. Patient in the stereotactic body frame at the Sahlgrenska University Hospital. The patient is immobilized using a vacuum pillow and the body frame is placed relative to the treatment machine using designated rulers.

The patient is positioned in the body frame and a pre-treatment CT scan is performed. The gross tumor volume (GTV) is then contoured on each axial slice in the TPS and the CTV is defined as the same volume as the GTV. To create a PTV, margins of 5 mm in the transversal plane and 10 mm in the cranio-caudal direction are added to the CTV. The treatment is delivered with 4–6 coplanar or non-coplanar 4-6 MV photon beams shaped with an MLC. This results in an inhomogeneous PTV dose distribution with central doses of 63-69 Gy as well as very steep dose gradients outside the PTV keeping the high-dose region small and the mean lung dose low (Figure 3.2, top). CT imaging was repeated before each fraction to verify the position of the tumour relative to the coordinate system of the body frame.

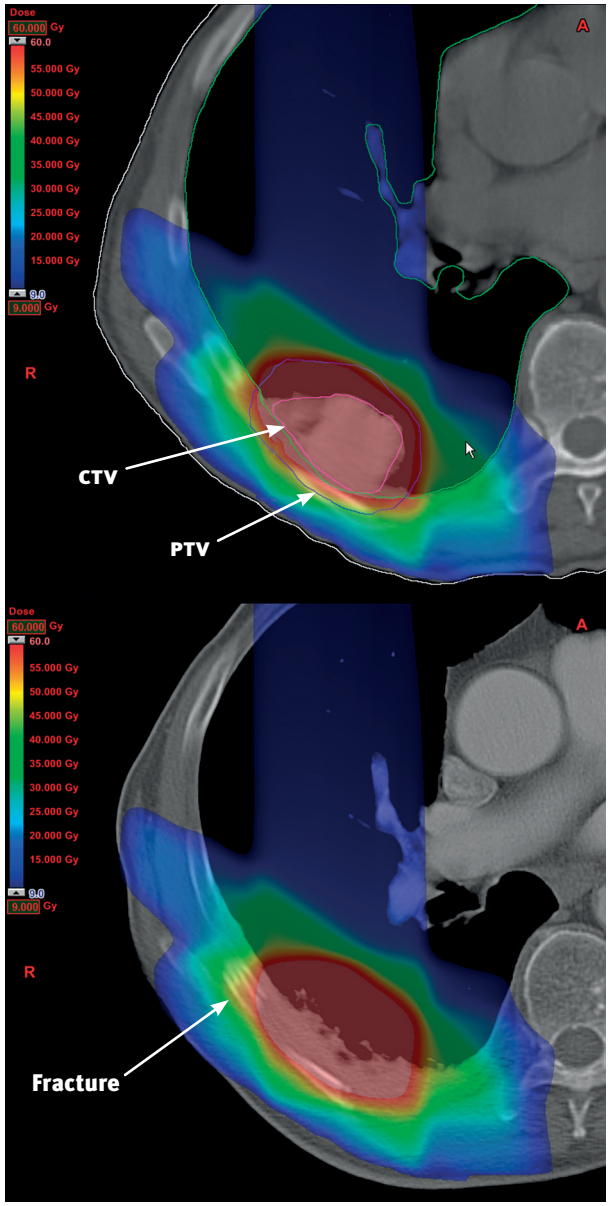

FIGURE 3.2. Top: Dose distribution in a transversal pre-treatment CT slice for an NSCLC SBRT patient. Bottom: Dose distribution superimposed on a follow-up CT.

3.1.4 NTCP modelling of radiation-induced rib fracture (Paper I)

All patients treated with SBRT were monitored after treatment with regards to both toxicity and tumour control. The follow-up included CT scans performed every 6 months. The endpoint for this work was radiation-induced rib fracture as verified by CT scan at any time after treatment (Figure 3.2, top). It should be pointed out the endpoint was

defined for each rib and some patients did experience multiple fractures (Table 1 in Paper I). In total, 13 rib fractures in seven patients were found close to the treatment volume and for which dose distribution data were available. All ribs receiving at least 3×7.0 Gy were separately contoured in the TPS. This resulted in 81 contoured ribs, 13 with and 68 without fracture, and the DVH for each rib was exported for analysis. Furthermore, CT scans for the patients containing the 13 fractured ribs were exported to the TPS and co-registered with the pre-treatment CT scans. This way we could determine which rib DVH that corresponded to which rib from the follow-up CT and assign the correct endpoint (0 for no rib fracture and 1 for rib fracture). The entire dataset is shown in Figure 3.3. Although the dose gradient outside the PTV is steep, some ribs are located within the PTV (Figure 3.2, bottom) and the maximum doses for those ribs are consequently higher than the prescribed dose of 45 Gy (Figure 3.3).

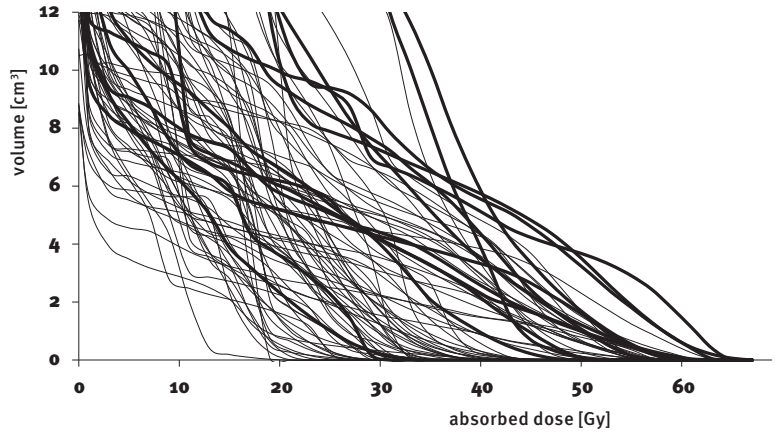

FIGURE 3.3. DVHs for ribs without (thin curves, n=68) and with rib fracture (thick curves, n=13) for 26 patients treated with SBRT.

Five different ways of summarizing each DVH into one descriptor value were used: cutoff volumes (D_{aV} and D_{rV}), cutoff doses (aV_D and rV_D), and the mean absorbed dose (see section 2.3.1.2 for definitions). Each descriptor was then used as input in dose- or volume-response curves to find the NTCP model that best described the risk of radiation-induced rib fracture.

The strongest association between dose and risk of rib fracture lay in the high-dose/small-volume region of the DVH. Both absolute and relative DVHs were assessed, but models for absolute volume provided better fits. The dose-response curve for D_{2cm^3} was described by D_{50}=49.8 Gy and $\gamma_{50,n}$=2.05 (Figure 3.4). This results in 10% risk of radiation-induced rib fracture for a total dose of 34 Gy when the treatment is delivered in three fractions. Using ROC analysis, the AUC was 0.82±0.07 (1 SEM), indicating a high predictive strength when using D_{2cm^3} as a dose descriptor in the model.

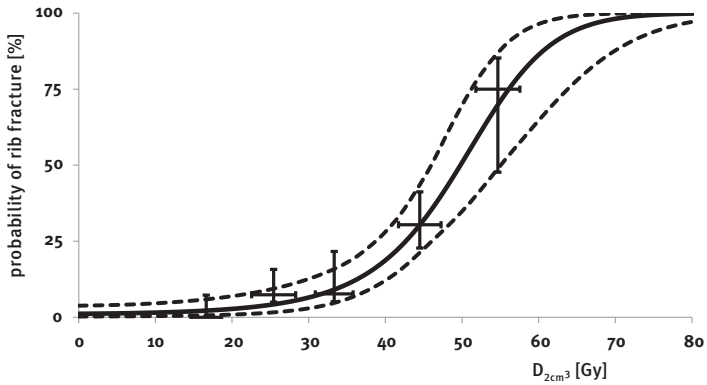

FIGURE 3.4. Dose-response curve for the relationship between the dose to D_{2cm^3} and rib fracture (solid curve) and the corresponding 68% CIs (dashed curves). The descriptor values have been binned into five groups to illustrate the observed rib fracture. The horizontal bars show mean±1 SD and the vertical error bars show 68% CI for the observed probability.

3.2 Prostate cancer - genitourinary toxicity (Papers II-V)

In 2008, a questionnaire surveying radiation-induced toxicity was sent out to all prostate cancers survivors treated with radiation therapy at the Sahlgrenska University Hospital during 1993 to 2006. The survivors had been treated with either primary EBRT, salvage EBRT following prostatectomy, or a combination of EBRT and HDR BT. A group of non-pelvic-irradiated men were also included in this study to provide information about symptom occurrence in population-based individuals (background rate). For each survivor, ten OARs were delineated on the EBRT pre-treatment CT, the dose distribution was reconstructed from treatment records and DVHs were exported. The BT OAR dose contribution could not be assessed from treatment documentation; this was addressed in Paper IV.

The questionnaire contained, among other things, 21 questions on genitourinary symptoms. The overall purpose of Papers II-V was to use the obtained dose distribution data for NTPC modelling of genitourinary toxicity data from this questionnaire. In Paper II, an overview of symptoms among survivors and controls was presented. NTCP modelling was performed for urethral pain and incontinence in Paper III and V, respectively. Of specific interest was to investigate how the large dose per fraction delivered with BT – 10 or 15 Gy – affected the outcome compared to men treated with conventionally fractionated EBRT.

3.2.1 Prostate cancer

Prostate cancer is the most common form of cancer among Swedish men with about 9700 men diagnosed each year [69]. Prostate cancer is also the leading cause of cancer-related death among Swedish men, with about 2400 yearly deaths [70]. The disease

becomes more common with age: in 2010 about half of newly diagnosed men were 70 years or older [69]. Various examinations such as serum markers of prostate-specific antigen (PSA), histological grade (Gleason score), and evaluation of disseminated disease are used to assist in choice of treatment strategy. If the disease is confined to the prostate, the major primary treatment options are surgery and radiation therapy modalities such as EBRT and BT.

3.2.2 Radiation therapy

Conventionally fractionated EBRT to a total dose of 60-70 Gy using non-conformal box techniques was initially used in the treatment of prostate cancer. This resulted in moderate tumour control, but high risks for urinary bladder and rectal toxicity due to large treatment volumes. At the same time, it was recognized that delivering higher doses to the prostate led to better local control [79]. With the introduction of CT-based 3D CRT, the dose to the prostate could be increased while simultaneously decreasing the volume of irradiated surrounding normal tissue; this led to lowered treatment-related toxicity [80, 81]. Image-guided techniques have enabled a further dose reduction in surrounding OARS [82].

About the same time as CRT was introduced in the 1980's, HDR BT for prostate cancer was developed in [43, 83, 84]. The BT was typically given as a boost added to standard EBRT.

The initial rationale behind using HDR BT was twofold: to be able to accurately treat the intended target volume and to utilize the steep dose gradients outside the target to irradiate less OAR volume [43]. This would potentially lead to an increased therapeutic ratio. Since each BT session is time-consuming (treatment procedure described below), the prescribed dose at each fraction was in the range of 8 to 15 Gy.

3.2.3 Fractionation sensitivity of prostate cancer

In 1999, Brenner and Hall published an analysis of the fractionation sensitivity of prostate cancer comparing conventionally fractionated EBRT with low-dose rate BT and arrived at an α/β value of 1.5 Gy [85]. Since then, several papers which confirm this result have been published [86-88]. The low tumour α/β value makes prostate cancer an ideal candidate for hypofractionated radiation therapy and several different treatment regimens have been suggested [89].

3.2.4 Radiation therapy for prostate cancer at the Sahlgrenska University Hospital

3.2.4.1 EBRT TECHNIQUE

The EBRT technique has basically been the same over the studied period, regardless if the treatment has been delivered as primary or salvage EBRT or as part of the EBRT+BT combination.

EBRT was individually planned based on CT imaging with the patient in a supine treatment position and with a low concentration of contrast in the bladder. Using these images, the CTV was defined as the prostate gland or, in the case of prostatectomized

patients, the post-operative prostatic region. The PTV was defined as the CTV with a 20-mm margin in all directions except posteriorly, where the margin was 15 mm or maximum half the rectal cross-sectional area. For all patients, a three-field 3D CRT technique with one anterior-posterior and two opposed lateral wedged fields was used. The shape of each field was individually optimized by either MLC or by using lead blocks. The photon beam quality was in most cases 15 MV, but 11 MV was used as well. The dose distribution was calculated with a pencil-beam algorithm and normalized in the centre of the PTV so that the 95%-isodose encompassed the PTV. For the primary and salvage EBRT groups, prescribed total EBRT dose was in most cases 70 Gy and for the EBRT+BT group 50 Gy, both at 2 Gy per fraction.

3.2.4.2 BRACHYTHERAPY TECHNIQUE

The HDR BT technique was early adopted at the Sahlgrenska University Hospital – first patient treated in 1988 - as

> *"[a]n alternative technique for the delivery of a high dose to a well defined volume with high precision and a rapid decrease of the dose to the surrounding organs is brachytherapy […]" [90]*

The regimen consisted of two HDR BT 10-Gy fractions separated by 14 days in the middle of 50 Gy EBRT. The total tumour dose was thus 70 Gy given in an OTT of 7 weeks. It was recognized that the high dose per fraction delivered to the prostate resulted in an advantageous higher tumour effect [91]. Borghede *et al.* calculated $EQD2_{10}$ = 83 Gy, but also hypothesized that the α/β value could be lower due to "*an underestimation of the repair capacity*" and calculated $EQD2_{6}$ = 90 Gy.

The brachytherapy procedure and the delivered dose distributions have been fairly similar during the studied period. A catheter filled with an air/gel mixture was introduced in 2000/2001 to better identify the urethra, and digital storage of ultrasound images and dose distributions began in March 2003.

At each brachytherapy session, the patient was placed in lithotomy position (Figure 3.5). Transversal images were captured every 5 mm from the base to the apex of the prostate using a transrectal ultrasound probe. The CTV was defined as the prostate gland and the PTV as the CTV with a margin of 2 mm in the transversal plane. The urethra was identified using the air/gel mixture and contoured with a diameter of 4 mm on each image. The dose distribution was optimized by determining needle positions and dwell times for the source within each needle, with the objective to cover the PTV with the prescribed dose (100%) while keeping the dose in the urethra lower than 120%. The treatment was delivered with a high-dose-rate ^{192}Ir source (treatment time 5-15 minutes), and the needles were removed immediately after treatment.

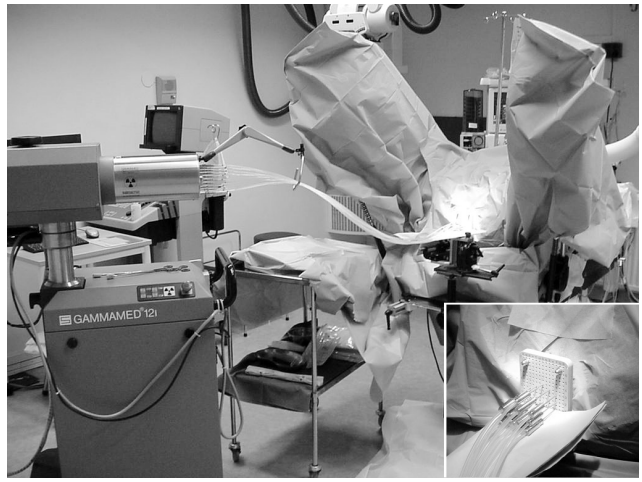

FIGURE 3.5. Patient in lithotomy position at brachytherapy. Needles have been inserted into the prostate through the perineum template and are connected to the afterloader.

3.2.4.3 DOSE DISTRIBUTIONS AND OAR DVH ACQUISITION

For all prostate cancer survivors participating in the study, the EBRT plans were identified in various databases used 1993-2006. If not already there, the CT images were transferred to the Eclipse treatment planning environment (Varian Medical Systems, USA) where the dose distribution in the original treatment plans were reconstructed from the treatment documentation. Ten relevant OARs in the pelvis were identified and consistently delineated. A total of 9501 DVHs were exported as text files, formatted to a suitable format using in-house developed software in JAVA and subsequently transferred to MATLAB (MathWorks Inc., USA) for quality control and analysis.

For all survivors treated with the combination of EBRT and BT, basic information on number of needles and TRAK were collected. For those treated with BT after March 2003 ultrasound images and dose distribution information were digitally available and additional data on the prostatic urethral mean and maximum doses could be retrieved. However, for all survivors treated with the combined therapy, the BT OAR dose distributions could not be recreated since the OARs of interest were outside the ultrasound field-of-view. This was addressed in Paper IV.

3.2.4.4 ESTIMATION OF COMPOSITE OAR DOSE DISTRIBUTIONS (PAPER IV)

To overcome the issue of missing OAR image information at BT, we suggested a method to estimate both the BT dose contribution and subsequently the composite EBRT+BT dose distribution. A subset of patients was randomly selected from the study population to implement the method. It was then applied to all 376 men treated with EBRT+BT.

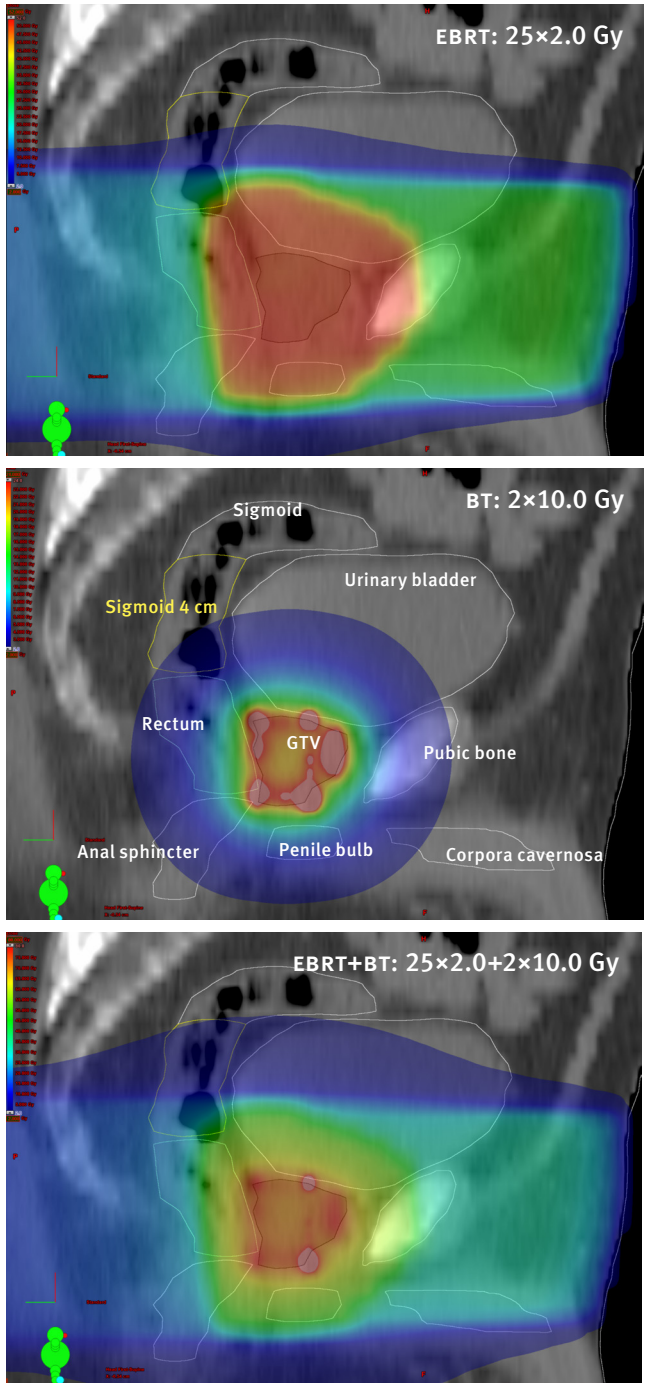

FIGURE 3.6. Absorbed dose distributions and OAR configuration in sagittal view (excluding the right and left femoral heads).
Top: 50-Gy EBRT;
Middle: 20-Gy BT reconstructed on the EBRT pre-treatment CT images;
Bottom: composite absorbed dose distribution, 70-Gy EBRT+BT.

Using this subset, the BT dose distribution and the composite dose distribution as well as their corresponding DVHs could be calculated. Since the same CTV was treated for both modalities and the dose outside the CTV was minimized to spare the OARs, the rationale behind the proposed method was that there could be correlations between the dose distributions from the EBRT and the BT (Figure 3.6). Likewise, there could be correlations between the DVHs from the EBRT and the BT. This was investigated to estimate four dose distribution descriptors that are useful in NTCP modelling of late effects: the near-maximum doses D_{2cm^3} and $D_{2\%}$, the mean absorbed dose and the fractionation-corrected mean dose. An exhaustive fitting of linear relationships between D_V (or V_D) from the EBRT DVH and the BT dose descriptor in question was performed to obtain the linear relationship with the highest coefficient of determination (R^2). The process is shown in Figure 3.7. In addition to using to D_V and V_D from the EBRT DVH to estimate the BT dose descriptor, its linear relationship (and corresponding R^2) with TRAK was also calculated.

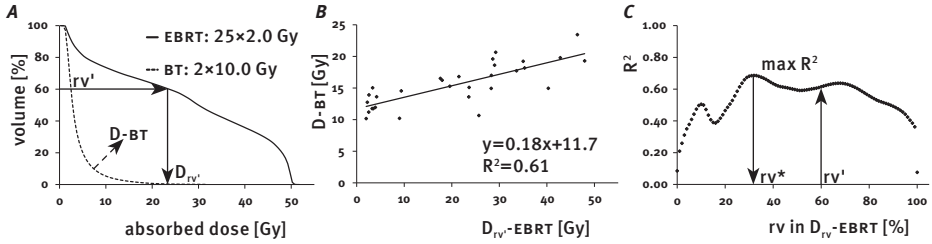

FIGURE 3.7. Illustration of the first step of the proposed method applied. In panel A, the $D_{rv'}$-EBRT value and the D-BT value are calculated for one patient. In panel B, the R^2 is calculated for the $D_{rv'}$-EBRT parameter values and the D-BT parameter values for all patients. This is repeated for all rvs and results in the R^2-graph shown in panel C. The maximum R^2 now determines the rv* value and the linear equation that best predicts the D-BT parameter.

The average R^2 for the investigated combinations of OAR and dose descriptor was 0.68±0.11 and 38⁄40 of all R^2 was larger than 0.5, that is, it was possible to find a well fitting linear relationship between the EBRT DVH and the BT dose descriptor in question.

TABLE 3.1. The model and associated parameter (cut-off) that best predicted the linear relationship for each sought BT parameter and its R^2 for the urinary bladder.

Organ at risk	Parameter	Model	Cut-off	R^2
Urinary bladder	$D_{2\%}$ (Gy)	D	rV=32.0 %	0.69
	D_{2cm^3} (Gy)	D_{aV}	aV=22.0 cm^3	0.66
	mean dose (Gy)	rV_D	D=31.5 Gy	0.84
	mean $EQD2_3$ (Gy)	rV_D	D=31.5 Gy	0.78

However, the final goal was the dose descriptor value for the composite EBRT+BT dose distribution. The composite mean dose (with or without fractionation correction) as

delivered by two different dose distributions (EBRT and BT in this case) is simply the sum of the respective mean doses. For the near-maximum doses the situation is not as straightforward. Addition of near-maximum doses by EBRT and BT can only be done when they are in the same anatomical location for both treatments. This was investigated by comparing the reference composite near-maximum dose given by the TPS to the dose obtained by addition of the EBRT dose (which we know) and the BT dose (which we have estimated). For the studied OAR dose distributions, the estimated composite near-maximum doses were found to be good approximations of the values calculated from the reference DVH (Table 3 in Paper IV). For such situations the composite value for any of the dose distribution descriptors for any similarly treated patient, can now be estimated from the EBRT DVH and the linear relationship. Furthermore, the fractionation-corrected composite dose can also be obtained by correcting the EBRT and BT doses for fractionation before addition.

3.2.5 Genitourinary toxicity and questionnaire

Patients undergoing radiation therapy for prostate cancer will as an unavoidable consequence have several pelvic organs irradiated. Among those are the urinary bladder, the urethra, the bladder neck and the trigone region, all being OARs from which genitourinary symptoms may originate [92]. It has also been suggested that patient-reported toxicity is the better way to report genitourinary toxicity since physician-reported toxicity may underestimate the actual symptom prevalence [92-94]. There is limited knowledge about late genitourinary toxicities with few dose-volume response relationships reported [92].

3.2.5.1 STUDY POPULATION

For the study population in Papers II-V, hospital records were used to identify all men that were at most 80 years old and treated with radiation therapy for localized prostate cancer between 1993 and 2006 at the Sahlgrenska University Hospital. The study included men who had not been diagnosed with distant metastases, had a sufficient knowledge of the Swedish language to read and understand written questions and were resident in Sweden at the time of follow-up. Furthermore, using the Swedish Total Population Register, 350 population-based controls matched for age and area of residence were identified; of those, 332 were not previously irradiated in the pelvic region and were invited to participate. The Regional Ethical Review Board in Gothenburg approved the project. To those who agreed to participate in the study, a questionnaire and a pre-stamped return envelope were sent out between February and November 2008.

Among the 1007 identified prostate cancer survivors, 985 agreed to participate and 874 (87%) returned a filled-in questionnaire. In the control group, 243 of 332 (73%) returned a filled-in questionnaire. The questionnaire contained questions on physical symptoms from the pelvic region, demographics, quality of life and comorbidities. For this work, a subset of 21 questions reflecting physical symptoms from the genitourinary region was used. The symptoms can be categorized into urinary obstruction, irritative toxicity and urinary incontinence. Four to seven answering categories were used to determine symptom intensity and occurrence where the lowest category corresponded to low intensity (e.g. a small amount urinary leakage) or few events (e.g. one event during the

last six months) and the highest category to high intensity (e.g. a large amount of urinary leakage) or several events (e.g. at every occasion).

There were three principal groups of prostate cancer survivors: those treated with primary EBRT, those treated with a combination of EBRT and HDR brachytherapy (EBRT+BT) and those treated with salvage EBRT following prostatectomy (POSTOP). The employed radiation treatment techniques for these survivors are described in section 3.2.4.

3.2.5.2 OUTCOME OF THE QUESTIONNAIRE (PAPER II)

Higher symptom rates (prevalence) among survivors compared to controls were found for twelve of the 21 investigated genitourinary symptoms: nine in the EBRT group, ten in the EBRT+BT group and five in the salvage EBRT group (Table 3.2). The prevalence for these symptoms in the control group, i.e. the background rates, varied between 1% and 30%. The pattern of symptom rates – the toxicity profile – was similar between the primary EBRT and EBRT+BT groups; the difference in prevalence was no more than 5 percentage points for any of the studied symptom. For the salvage EBRT group, only symptoms reflecting incontinence had significantly higher prevalence than the control group. Also, in this group, the prevalence of symptoms reflecting urinary flow was significantly lower than for the control group (i.e. the actual removal of the prostate gland seem beneficial in this regard).

TABLE 3.2. Prevalence for 3 of the 21 investigated genitourinary symptoms among the prostate cancer survivors treated with EBRT, EBRT+BT or salvage EBRT and the non-pelvic-irradiated control men. Prevalence ratios for the treated groups with respect to controls.

Treatment group *Symptom*	**EBRT** *n./N. (%)* *PR (95% CI)*	**EBRT+BT** *n./N. (%)* *PR (95% CI)*	**POSTOP** *n./N. (%)* *PR (95% CI)*	**CONTROL** *n./N. (%)* *PR (95% CI)*
5. Sensation of bladder being non-empty after urinating on half or more of the occasions	62/297 (21) 1.4 (1.0*-2.1)	81/368 (22) 1.5 (1.1-2.2)	28/196 (14) 1.0 (0.6-1.6)	35/241 (15) Reference
15. Urethral pain when urinating on half or more of the occasions	10/298 (3) 1.4 (0.5-3.7)	23/368 (6) 2.5 (1.0**-6.1)	8/197 (4) 1.6 (0.6-4.6)	6/242 (2) Reference
16. Weekly urinary leakage, more than a few drops	68/298 (23) 2.0 (1.3-3.0)	67/368 (18) 1.6 (1.0**-2.4)	66/196 (34) 2.9 (2.0-4.3)	28/242 (12) Reference

POSTOP = salvage radiation therapy after surgical prostatectomy; PR = prevalence ratio; CI = confidence interval.
*, lower 95% CI below 1.0.
**, lower 95% CI above 1.0.

The temporal pattern of symptom occurrence varied, but the prevalence generally changed moderately over time. For all symptoms but one (nocturia), survivors with time to follow-up shorter than 3 years had a higher symptom rate than survivors with time to follow-up between 4 and 5 years.

3.2.6 Urethral pain (Paper III)

The question on urethral pain (question 15) had a statistically significant higher prevalence in the EBRT+BT group than in the control group and it was also notably higher than in the primary EBRT group. This in combination with the exposed location of

the urethra inside the target volume led to a more thorough analysis of the non-treatment-related and treatment-related factors impacting the occurrence of urethral pain after radiation therapy.

The (translation of the) studied question is "*The last 6 months, have you felt burning pain in the urethra when urinating?*" with the answering categories "*No*", "*Yes, less than half of the times*", "*Yes, about half of the times*", "*Yes, more than half of the times*", and "*Yes, always*". The endpoint was defined as "*No*" versus any occurrence.

The dose distribution along the urethra is schematically shown in Figure 3.8. The part of the urethra inside the prostate (the prostatic urethra) will receive a homogeneous dose distribution with a mean absorbed dose close to the prescribed dose for the EBRT treatment. Extracting data from the urethral BT DVH for all survivors having available dose distribution and image information (survivors treated after March 2003) showed that also the BT urethral dose distribution was fairly homogeneous. That the average mean dose was 106±3% (1 SD) and the average maximum dose was 111±3% (1 SD) of the prescribed BT dose. Survivors who had undergone radical prostatectomy have no prostatic urethra and were excluded from the analyses.

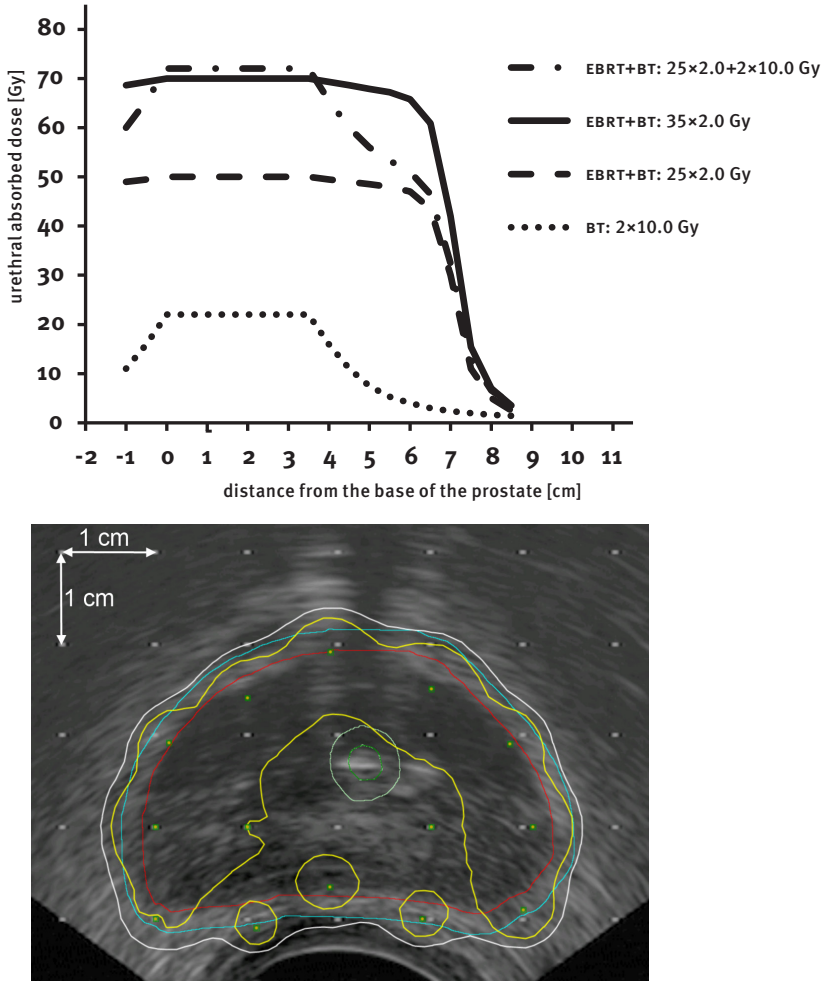

FIGURE 3.8 Top: Schematic description of the urethral dose distribution in cranio-caudal direction for 70-Gy EBRT and 70-Gy EBRT+BT. The prostatic urethral absorbed dose from EBRT is equivalent to the prescribed dose and the absorbed dose from BT is 106% of the prescribed dose.
Bottom: A transversal ultrasound image of the prostate with the prostate (CTV) in red, PTV in cyan, urethra in dark green, and expanded urethra in light green. Shown isodoses are 10 Gy (prescribed dose) in white and 12 Gy in yellow.

The prevalence of urethral pain was 24% among the EBRT+BT survivors compared to 13%, 11% and 12% among the primary EBRT, salvage EBRT and non-irradiated controls, respectively. Time to follow-up was the only non-treatment related factor that affected the prevalence of urethral pain for non-surgically-treated survivors. For survivors treated with 70-Gy EBRT+BT there seemed to be symptom relief over time: 32% versus 19% for time to follow-up shorter and longer than 3 years, respectively (Figure 2 in Paper III).

The time effect was taken into account by performing analyses separately for short and long follow-up (<3.0 years and ≥ 3.0 years). The evaluations were performed for the

mean urethral dose without fractionation correction and with fractionation-correction using the LQ model with α/β=3 Gy and the LQ-L model with α/β=3 Gy and d_t=8 Gy. For absorbed dose, no relationship between urethral dose and pain was found for either short or long time to follow-up. Relationships between irradiation and pain for long and short follow-up was found for LQ corrected doses when α/β=3 Gy was used, and no other choice of α/β did significantly improve this fit (Figure 3.9). For the LQ-L model, a dose-response relationship was found for long follow-up, but not for short. Using lower α/β or a higher d_t would however have confirmed a dose-response relationship in this situation as well.

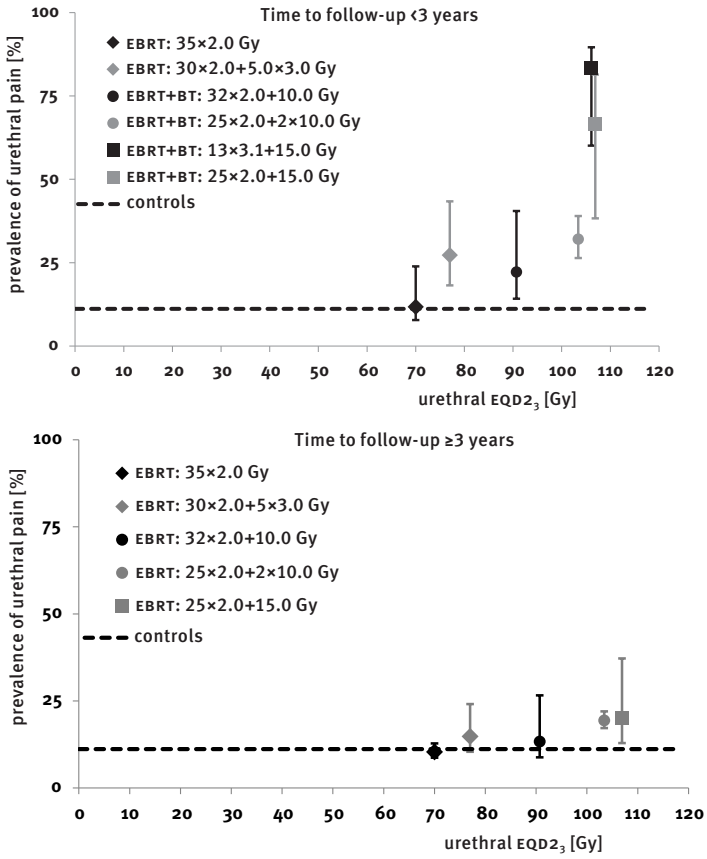

FIGURE 3.9. Prevalence of urethral pain for the different treatment groups stratified by time to follow-up. Top: time to follow-up shorter than 3 years. Bottom: time to follow-up longer than 3 years. The vertical error bars show the 68% CI for the observed prevalence.

For survivors treated with 70-Gy EBRT+BT, we also investigated if TRAK, number of needles, and irradiated length of the urethra was associated with an increased symptom risk. Specifically the irradiated urethral length was of interest since an association would point toward a volume effect. However, neither of the investigated factors was found to influence the occurrence of urethral pain.

Given sufficient time for symptom relief, the urethra has a high tolerance to irradia-

tion. Equieffective doses $EQD2_3$ below 90 Gy seem well tolerated, that is, the prevalence among survivors was equal to the background rate among non-irradiated individuals. The exposed anatomical location of the urethra makes it difficult to reduce the urethral dose without simultaneously reducing the tumour dose (and potentially jeopardizing tumour control), especially for EBRT techniques. For HDR brachytherapy, however, there are more possibilities for urethral dose reductions with only a small effect on the tumour dose, but it is also easier to irradiate the urethra with an unnecessarily high dose.

3.2.7 NTCP modelling of genitourinary toxicity (Paper V)

In this work, we used an NTCP modelling approach to further investigate the 21 genitourinary symptoms reported in Paper II. We used treatment and symptom data for 641 men treated with either primary EBRT or EBRT+BT as well as symptom data collected from 242 men in the control group.

The dose descriptors used for modelling purposes was 1) the prescribed dose, 2) the bladder mean dose and 3) the bladder near-maximum dose defined as D_{2cm^3} and $D_{2\%}$ as well as $EQD2_3$ versions of 1-3 using the LQ model and α/β=3 Gy. The prescribe dose can be considered representative of the urethral dose and the bladder near-maximum dose is representative of both the trigonal region dose and the bladder neck dose. Symptoms were primarily used with the cut-offs that were deemed clinically relevant. We also examined secondary cut-offs at one level above and one level below the primary cut-off to balance high background rates against too few events among survivors.

To establish that a dose descriptor was associated with the symptom, two criteria had to be fulfilled: the descriptor had to be statistically significant in logistic regression and the symptom prevalence among survivors had to be significantly higher than among controls. Analyses were separately performed for the group of survivors treated with primary EBRT and for the group treated with EBRT+BT. For survivors treated with EBRT+BT, the method in Paper IV was used to estimate composite doses. However, assuming the same amount of bladder filling, 300 cm^3, at every BT irradiation, all survivors were assigned the same mean urinary bladder dose contribution from BT: 1.6 Gy per 10-Gy fraction (absorbed dose), 2.0 Gy per 10-Gy fraction ($EQD_{mean}2_3$), and 3.7 Gy per 15-Gy fraction ($EQD_{mean}2_3$). This assumption was founded in the consequences by standard routines foregoing BT where the urinary bladder was emptied before planning and needle insertion resulting in similar bladder filling between patients at treatment.

The only symptom found to be relevant for NTCP modelling was urinary incontinence (question 16 in Table 3.2). Among the men treated with primary EBRT, both urinary bladder mean dose and fractionation-corrected urinary bladder mean dose correlated with this symptom.

Using survivors treated with primary EBRT in 2-Gy fractions (n=241), dose-response curves were estimated, Figure 3.10. The dose-response curve for fractionation-corrected mean dose (bottom panel) was parameterized by $EQD2_3$ = 89.0 Gy and γ_{50}= 1.06 using a background rate of 7% for EBRT survivors receiving their treatment with a varying number of 2-Gy fractions. This means that if the $EQD_{mean}2_3$ can be kept below 35 Gy, the excess risk is estimated to less than 5%.

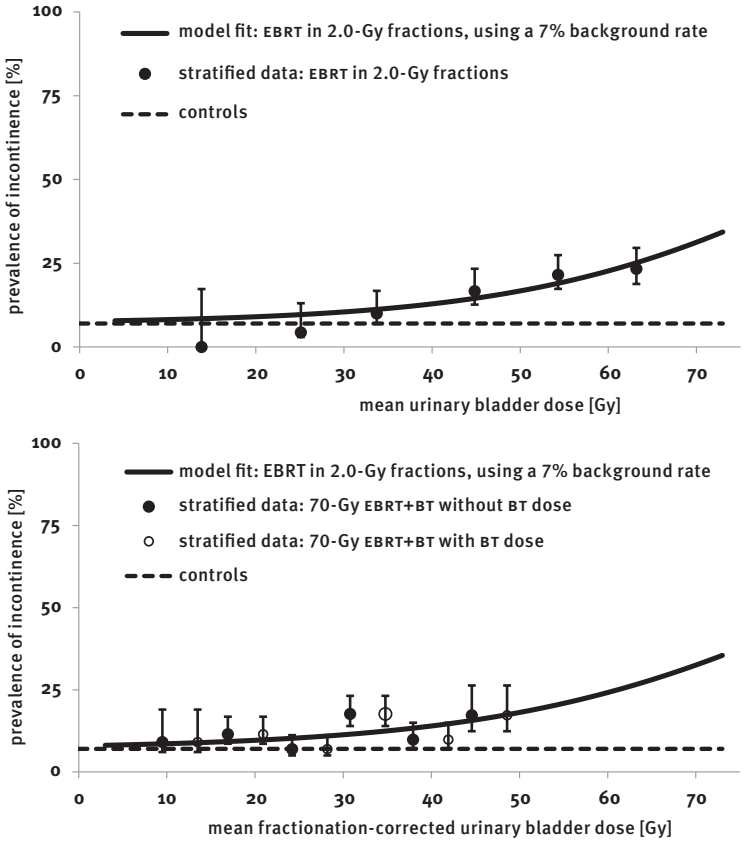

FIGURE 3.10. Top: Dose-response curve for prevalence of incontinence using mean urinary bladder dose and a 7% symptom background rate.
Bottom: Dose-response curve for prevalence of incontinence using mean fractionation-corrected urinary bladder dose and a 7% symptom background rate. The mean doses have been stratified into six bins; the vertical error bars show the 68% CI for the prevalence.

4. DISCUSSION

The presented results in Papers I-V cover methodological and practical issues such as radiobiologically consistent mathematical descriptions of dose-response curves, dose-distribution estimation in situations with limited treatment information and how to manage situations where non-treatment-related factors contribute to the studied toxicity. These principles were applied in two different clinical datasets from patients treated at the Sahlgrenska University Hospital. In Paper I we found dose- and volume-response relationships for radiation-induced rib fracture after hypofractionated SBRT. In Papers II, III and V we evaluated and compared genitourinary toxicity after conventional and hypofractionated radiation therapy for prostate cancer and also found dose-response relationships for urethral pain and urinary incontinence.

4.1 Radiation-induced rib fracture after hypofractionated SBRT for NSCLC (Paper I)

4.1.1 NTCP modelling of radiation-induced rib fracture

The dataset in this study has several strong features. All treatments were planned based on CT imaging in a group of consecutive patients and the high-precision patient setup in the stereotactic body frame meant that the calculated DVHs can be considered accurate descriptions of the delivered rib dose distributions. The studied endpoint could be thoroughly determined: the status of all ribs in the chest could be evaluated with high sensitivity and specificity using the frequently performed CT scans. Furthermore, the status of the ribs prior to irradiation was available in the pre-treatment scan.

One drawback of the study is the limited number of rib fractures (n=13) which leads to parameter estimates with wide confidence intervals. Another issue is the limited follow-up time in some patients; those without rib fracture with short follow-up may present with a fracture at a later time. This would lead to an underestimation of the risk. A great majority of rib fractures occur within 4 year after treatment and the median follow-up among the non-fractured ribs in our study was 27 months [95-97].

The dose distribution was calculated with a pencil-beam algorithm. This is known to give erroneous results in lung tissue [98-100]; we estimated its accuracy in the ribs to be within 5%. Furthermore, the pencil-beam algorithm calculates the absorbed dose to water in the medium in question and not the absorbed dose to the medium; the difference is about 10% in cortical bone [101].

This was, to our knowledge, the first paper that used clinical data for NTCP modelling of late effects in highly hypofractionated radiation therapy for any endpoint. Several papers on radiation-induced rib fracture after hypofractionated radiation therapy have been published since, although only a few with endpoint and OAR definition similar to ours [95-97]. The treatment techniques in the these studies varies, photon EBRT in four fractions to 48 Gy [95], proton EBRT in six fractions to 60 Gy [96] and photon EBRT in three-four fractions to 30-60 Gy [97]. The conclusions are overall analogous to ours

as the high-dose/small-volume region of the DVH correlates stronger with rib fracture than a low dose in a large volume.

4.1.2 Dose-response curves for hypofractionated radiation therapy

Radiobiologically consistent dose-response curves to be used when a treatment is delivered with a fixed number of fractions were derived using α/β from the LQ model to quantify the fractionation sensitivity. As purely mathematical entities they contain no uncertainties *per se*, but it cannot be guaranteed that they accurately describe actual clinical dose-response relationships. When fitted to the rib fracture dataset, all values of α/β resulted in equally good fits. This may seem somewhat surprising, but it is actually advantageous since we do not need to know the correct α/β value to estimate the dose-response curve parameters. When reporting results for dose-response relationships, or when applying dose-response curves reported in the literature, it is important to be aware of that incorrect handling of fractionation-effects may lead to incorrect results. Specifically, both the position (D_{50}) and the steepness (γ_{50}) are affected by the fractionation effect.

4.2 Genitourinary toxicity after radiation therapy for prostate cancer (Papers II-V)

4.2.1 Questionnaire and measurement of toxicity

The measurement of genitourinary toxicity for prostate cancer survivors and an age- and residency-matched control population were performed with a postal-based questionnaire. The questions were developed to measure clearly defined atomized symptoms. The symptom rates (prevalence) among prostate cancer survivors were compared to the background rates among the non-pelvic-irradiated men in the control group which assisted in deciding whether a symptom could be attributed to the treatment or was due to other factors.

The strengths of this study are that the investigation was performed in an unselected large population with long follow-up and a high response rate (87%), that atomized patient-reported symptoms were used, and that symptom background rates from a population-based, matched control group could be used for comparison [92, 93]. We could reconstruct the EBRT urinary bladder DVHs for 96% ($^{841}/_{874}$) of the study participants. The mean bladder dose contribution from BT, however, could not be reconstructed from treatment documentation but had to be estimated.

We lack information on pre-treatment morbidity which previously has been shown to be associated with the risk of late genitourinary toxicity [92, 102]. However, pre-treatment prostate enlargement or the presence of cancer may cause this morbidity, which is not seen among ”healthy” controls [103]. Therefore, one may assume that the symptom rates in population-based controls represent an optimal level for post-treatment comparison.

Interpretation of the effect measures was used with epidemiological methods as adapted to the cancer survivorship field by the hierarchical step-model for causation

of bias [50]. According to this, there are different sources of error that can threaten the validity of a study such as confounding, misrepresentation and misclassification.

4.2.1.1 CONFOUNDING

A confounder is a variable that is casually related to the independent variable (X) and the dependent variable (Y). If not adjusted for in the analyses, a confounder can produce a mis-estimation of the strength of association between X and Y. We can only evaluate the potential confounders for which we have data. In this study, the questionnaire contained questions on possible confounders such as age, body mass index (BMI), and comorbidities to enable adjustment of these factors in the analyses if necessary.

Age is a potential confounder for OAR dose (X) when genitourinary toxicity (Y) is evaluated. Age-adjusted prevalence ratios were calculated for the genitourinary toxicity profiles in Paper II, but did not effect the overall conclusions.

4.2.1.2 MISREPRESENTATION

Misrepresentation occurs when participants differ from non-participants in some crucial way. For instance, if men experiencing late genitourinary symptoms are non-participants to a higher degree than men not experiencing these symptoms, we will underestimate the symptom prevalence. If non-participation due to symptom occurrence differs between the survivors and the controls, the calculated prevalence ratio will be affected. The information from non-participants will remain unknown and a large loss to follow-up will seriously affect the validity of the effect measures. The only way to minimize misrepresentation is to keep the participation rate as high as possible.

In this study, 874 of 1007 (87%) identified men returned a filled-in questionnaire; among the controls meeting the inclusion criteria, 243 of 332 (73%) returned a filled-in questionnaire.

4.2.1.3 MISCLASSIFICATION

Misclassification is the same as measurement error and can concern either the exposure or the outcome under study. There are two types of misclassifications: non-differential and differential. Non-differential misclassification occurs when the probability for committing a measurement error is the same for all participants in a study irrespective of exposure or outcome. Committing such errors will generally shift the prevalence ratio towards 1, i.e. towards no effect. Differential misclassification occurs when the probability to commit a exposure or outcome measurement error is different in various groups of the study population. Committing such errors will affect the effect measure in unpredictable ways.

Great care was taken in the construction of the questionnaire (for instance through face validation) to minimize the risk of misclassification. However, the participants can introduce misclassification when trying to remember a symptom and report an overestimated or underestimated symptom occurrence. Mistakes can also be made during the manual transferral of the filled-in questionnaire into digital format. Differential misclassification may be an issue in the estimation of mean urinary bladder doses in Paper V where the BT mean dose contribution had to be estimated using methods from Paper IV. This potential source of misclassification was addressed by performing analyses separately in the EBRT and EBRT+BT groups.

4.2.2. Survey of genitourinary late toxicity (Paper II)

This was a survey of the collected questionnaire data. Survivors were stratified according to treatment modality and prevalence and prevalence ratios with respect to controls were calculated for each group.

We found that survivors in the EBRT and EBRT+BT groups had similar toxicity profiles. For survivors treated with salvage EBRT, symptoms reflecting incontinence were the most common; this is a well-known toxicity after prostatectomy although some cases can be attributed to the EBRT [104-106]. Symptom background rates, or occurrences of symptoms in a population similar to the one under consideration, become more important to acknowledge when estimating risks for "less severe" toxicities. If the background rate is substantial and overlooked, the toxicity induced by the treatment will be overestimated. Modifying the dose distribution may then lead to a jeopardized tumour control without actually lowering the symptom risk as much as anticipated.

The reports on temporal pattern of genitourinary symptoms are diverging in the literature. Symptoms reflecting obstruction, urgency and frequency have been reported to remain at the same level with time [107, 108] whilst incontinence is typically reported to increase [105, 109, 110]. In our study, the symptom prevalence tended to be higher the first years after radiation therapy and then decreased. The exception was for urinary frequency that increased with longer time to follow-up. Genitourinary toxicity has previously been reported to decrease over time and it has also been suggested that the actuarial incidence may overstate the toxicity in the long-term perspective [110].

4.2.3 Urethral pain (Paper III)

After observing that burning urethral pain during urination was a symptom that was more prevalent among survivors treated with EBRT+BT than among primary EBRT survivors, we investigated how treatment-related and non-treatment-related factors impacted the prevalence.

We found that prostate cancer survivors treated with EBRT+BT reported a higher occurrence of urethral burning pain during urination compared to those treated with primary and salvage EBRT. The symptom was more common among men with 3 years to follow-up compared to men with more than 3 years to follow-up. This observation of symptom relief is in line with previous reports for similar treatments [110].

We demonstrated dose-response relationships where higher urethral EQD23 values corresponded to a higher occurrence of pain explaining the differences in prevalence of pain for the various primary EBRT and EBRT+BT fractionation regimens. Our dataset is to about 85% comprised of survivors treated with either 35×2.0-Gy primary EBRT or 25×2.0+2×10.0-Gy EBRT+BT, that is, we have relatively little symptom risk information for other dose levels. This lack of data for many different urethral doses has the effect that we could not isolate a small range of α/β values that better describe the observed outcome, although we could conclude that using fractionation-corrected dose gave better fits than using absorbed dose.

The symptom rate among survivors treated with primary 70-Gy EBRT (regardless of time to follow-up) was no different than the symptom rate among the controls. Waiting for symptom relief to occur during three years after treatment, even $EQD2_3$=90 Gy seem to be well tolerated. One observation is that among survivors that were treated with

'double hypofractionation', 13×3.1+15.0-Gy EBRT+BT, 5/6 (83%) reported urethral pain. The time to follow-up among those men were short, 1.3-2.0 years, and this prevalence can be compared to 9/23 (39%) among survivors treated with 70-Gy EBRT+BT having the same time to follow-up (prevalence ratio=2.1; 95% CI 1.1-4.0). There was an advantage of having access to symptom data from non-pelvic-irradiated men. The 10% prevalence among survivors treated to 70-Gy primary EBRT - similar to the background rate of 11% - could otherwise easily been attributed to the treatment.

4.2.4 Composite dose distributions for combined EBRT and BT (Paper IV)

For all 373 survivors treated with the combination of EBRT and BT, none of the ten defined OARs in the pelvis were in the field-of-view of the ultrasound probe during BT. This meant that we had neither direct information of the dose contribution from the BT nor of the composite dose distribution. The purpose of this study was to suggest and use a method that in a time-efficient way can estimate the brachytherapy dose contribution as well as the composite dose distribution to facilitate NTCP modelling. The dose descriptors judged to be of interest in the modelling of late effects was the mean dose, the fractionation-corrected mean dose, and the near-maximum doses D_{2cm^3} and $D_{2\%}$.

The utility of the method depends on two things: can it be successfully implemented and are the estimated doses good approximations of those actually given at treatment? In the dataset explored in this work, high R^2 values were obtained in most of the OAR and BT parameter combinations and the composite dose descriptor values were judged to be useful as well. The steep dose gradient outside the PTV delivered by the BT has two main consequences. First, OARs located far from the PTV are located in a region with a shallow dose gradient and will also receive a small dose contribution; a mis-estimation of this small contribution will not be critical. Second, the OARs close to the PTV are located in a region with a steep dose gradient and will also be subject to a higher BT dose; a mis-estimation in this case will introduce a larger error in terms of absolute dose. Also, for OARs close to the PTV, the steep dose gradient will have the consequence that differences in the PTV- and OAR-definitions will greatly affect the shape of the calculated DVHs.

Furthermore, if the determined relationship between the EBRT and BT DVH parameters is to reflect what actually is delivered by BT, there must be a similarity in OAR and PTV configuration at both treatments. This must be judged on an OAR-to-OAR basis.

4.2.5 NTCP modelling of genitourinary toxicity (Paper V)

The purpose of this study was to perform NTCP modelling of genitourinary toxicity after radiation therapy for prostate cancer.

We found a dose-response relationship between urinary bladder mean dose (with or without fractionation correction) and urinary incontinence among survivors treated with primary EBRT. We believe that the reasons for not finding this relationship between mean bladder dose and incontinence in the 70-Gy EBRT+BT group may be explained by some additional effect by the BT or that the 5% excess risk was too small to detect. However, it is worth noting that on a group level, the model predictions for the EBRT+BT group with and without the estimated BT contribution were 13% and 14%, respectively; both close to the observed incontinence prevalence (12%) in the EBRT+BT.

Interestingly, the high prevalence for the 60-64+10-Gy EBRT+BT regimen (7/24, 29%) and the low incontinence prevalence in the 58-60+15-Gy EBRT group (2/38, 5%) are not satisfactorily explained by the mean urinary bladder dose; this needs to be further investigated.

The urinary bladder is a highly flexible organ and its size changes with filling. For EBRT, this means that unless a patient has the same amount of filling at a specific fraction as he had at the pre-treatment CT, the calculated DVH will not be a good representation of a delivered dose distribution at that fraction. However, if pre-treatment CT imaging captures the average bladder filling expected over the whole course of radiation therapy, both the mean and near-maximum doses can be considered reasonably accurate.

4.3 General remarks

The LQ model is currently the established way to take the fractionation effect into account. However, currently we lack clinical evidence for the validity of the LQ model at high doses per fraction but even if the model turns out to be valid, we may not know the relevant α/β values. This impairs our ability to design optimal hypofractionated treatment regimens where both tumour control and normal tissue toxicity are considered.

How the lack of knowledge of α/β affects NTCP modelling of late toxicities in fractionated radiation therapy depends on the treatment regimen. If all patients are treated with the same number of fractions and each patient is treated with the same dose per fraction throughout the treatment, dose-response curve parameter estimations are insensitive to the value of α/β; this was utilized in Paper I. This is in contrast to the dose-response relationship for urethral pain in Paper III where the urethral dose for the combination of EBRT and BT was delivered with different doses per fraction. Consequently, fractionation-corrected doses had to be used to assess how irradiation affected the prevalence of urethral pain leading to α/β-dependent estimates of tolerance doses.

Although the fractionation sensitivity may be a major concern for NTCP modelling in hypofractionated radiation therapy, the volume effect also needs to be considered. In the analysis of rib fractures in Paper I, cut-off descriptors were used to summarize the DVH into one value representing the entire dose distribution. The high-dose/small-volume region was associated stronger with rib fracture than a low dose in a large volume indicating that ribs have a small volume effect. In the analysis of urethral pain in Paper III, the BT urethral dose distributions were fairly homogeneous, i.e. there was little difference between the mean and maximum dose making it difficult to detect any potential volume effects. The length of irradiated urethra was also examined, but no relation between the irradiated length and occurrence of pain was found. In the search for dose-response relationships of various genitourinary symptoms in Paper V, four dose distribution parameters representing the dose distribution in OARs hypothesized to be relevant for genitourinary toxicity, were used (or eight, since each parameter was analysed with and without fractionation correction). The urinary bladder was the only OAR where we evaluated potential volume effects. We found an association between the urinary bladder mean dose and the prevalence of urinary incontinence, but not for the near-maximum dose.

5. CONCLUSIONS AND FUTURE PERSPECTIVE

5.1 Conclusions

In this thesis, the focus has been on modelling late toxicity following hypofractionated radiation therapy. The main conclusions are:

- Radiobiologically consistent mathematical expressions of dose-response curves in a treatment situation with a fixed number of fractions must consider the fractionation sensitivity; such equations were derived in Paper I using α/β from the LQ model. It was shown that although an α/β value needed to be included, equally good fits could be achieved regardless which value was chosen. However, when applying a known dose-response curve for another fractionation regimen, both D_{50} and γ_{50} are affected and must be recalculated to fit the new situation.
- The risk of radiation-induced rib fracture after hypofractionated SBRT could be estimated using dose-response curves and information from the DVH. The high-dose/small-volume region of the DVH was more strongly associated with rib fracture than a low dose in a large volume.
- A time-efficient method to estimate the composite mean and near-maximum doses in ten OARs in the pelvis after combined prostate EBRT and HDR BT was proposed and implemented. The steep dose gradients delivered by BT will sometimes make estimations for OARs close to the PTV uncertain while estimations for OARs further away will be more robust.
- The toxicity profiles for genitourinary symptoms were similar for prostate cancer survivors treated with conventionally fractionated EBRT and those treated with a combination of conventionally fractionated EBRT and HDR BT. The corresponding symptom rates among non-pelvic-irradiated control men varied substantially.
- Prostate cancer survivors with 3 years to follow-up reported urethral pain more frequently than survivors with more than 3 years to follow-up. A relationship where higher urethral $EQD2_3$ corresponded to higher prevalence of pain was demonstrated; no such relationship was seen for absorbed dose.
- The mean urinary bladder dose, with or without fractionation correction, was a significant predictor of incontinence among prostate cancer survivors treated with primary EBRT.

- Having access to symptom data from non-pelvic-irradiated men was advantageous for modelling of genitourinary toxicities: symptom rates among survivors could be set in relation to the background rate preventing us from overestimating the effect of irradiation.

5.2 Future perspective

There is now a substantial amount of available data on radiation-induced rib fracture after hypofractionated SBRT. These data have large variation in both number of delivered fractions and in dose per fraction. If these data were pooled, they may give some insight into the validity of the LQ model at high doses per fraction for this late toxicity.

Hypofractionated radiation therapy regimens are becoming an established treatment for localized prostate cancer and they have the potential to deliver a high equieffective dose using EBRT or HDR BT. It is reasonable to believe that both hypofractionated EBRT and HDR BT will continue to be used with image-guided techniques and small CTV-to-PTV margins, resulting in small volumes of normal tissue irradiated to high doses and also a low mean urinary bladder dose. However, normal tissues within the PTV will be subject to a non-ideal situation of high doses at high doses per fraction. Current knowledge about which OAR (or group of OARs) that is responsible for a specific genitourinary late toxicity is limited. This situation can only be improved by collecting and analysing high-quality toxicity and dose distribution data.

Radiation therapy delivered by different modalities or by multi-phase EBRT results in an OAR being irradiated with different dose distributions. This has the effect that even if the voxel-wise sum of the absorbed dose distributions and its corresponding DVH can be calculated by the TPS, this DVH cannot be used to correct for fractionation effects. However, we are approaching a situation where commercially available TPSs can add dose distributions from different modalities and calculate DVHs for the fractionation-corrected dose distribution. This will most likely be used in both the optimization of treatment plans and for NTCP modelling purposes.

Dose distributions in the OARs from today's hypofractionated radiation therapy are delivered with high doses per fraction and may be exceptionally inhomogeneous. It should be recognized that the two most widely used NTCP models, the LKB model and the relative-seriality model, have not yet been fitted to clinical data under those circumstances. Furthermore, although both may be used with fractionation-corrected DVHs, we do not know if they will result in reasonable parameter estimates when the input data looks decidedly different than before. This needs to be further investigated.

Prostate cancer, NSCLC, cervical cancer, and liver cancer are but a few examples of cancer types that can be expected to increasingly be treated with curative intent utilizing hypofractionated radiation therapy. As we continue to increase local control and overall survival for these patients, knowledge about how to design fractionation regimens and dose distributions that offer an optimal compromise between tumour control and toxicity becomes essential to maintain the quality of life both in the short term and long perspective

6. ACKNOWLEDGEMENTS

THE FIRST PERSON I want to thank is my supervisor **Karl-Axel Johansson** for his invaluable experience, keen eye for what truly is relevant, analytical mind, and for always gently pointing me in the right direction. A special thanks for always staying positive and not giving up on me during this long period; at last, you can spend more time orienteering and cross-country skiing.

Besides being an inspiring joint explorer in modelling and data interpretation, my co-author and also last-minute assistant supervisor **Caroline Olsson** has been an invaluable guide to the art of scientific writing. It is embarrassing how often her saying "But tell me what you mean!" followed by "But write that then!" have helped. Liquorice, coffee and laughter are always close when Caroline is around.

Co-author **David Alsadius** is greatly appreciated for the steady stream of new ideas, general support and help with data interpretation. **Gunnar Steineck** contributed greatly by having an uncanny ability to ask the right question and for giving precise and helpful advice. **Ulrica Wilderäng** was instrumental in carrying out endless analyses and re-analyses, and in keeping track of the overwhelming amount of data. Advice from expert biostatistician **Susan Tucker** at MDACC has been abundant, and her natural friendliness and helpfulness made my Houston stay memorable. Co-author and assistant supervisor **Jan Nyman** shared his clinical experience and offered useful manuscript comments.

I am grateful that my **colleagues** at therapeutic radiation physics for sharing their treatment planning skills and general knowledge about radiation therapy and radiation physics with me. Special thanks go to **Lena Marie Lundberg** and **Emma Djärv** for going the extra mile and making it possible for me to finish this work. The ability of current and former bosses to create practical solutions has been necessary and is appreciated.

All fellow **PhD students**, current and former, for discussions on and distractions from research; the coffee room is really the place to be. **Magnus Båth**, **Tom Bäck**, **Åsa Carlsson**, and **Nils Rudqvist** for advice, friendship and perspective, but even more for knowing and understanding the psyche of the PhD student. Thanks to all my friends outside the hospital and especially to **Johan Malmgren**, who besides being a great friend more than half my life, whose efforts with designing the thesis has been invaluable: obsessiveness at its finest!

And, finally, my heartfelt thanks go to my **family** for their unconditional support and encouragement; without it, everything else would be in vain. I look forward to seeing you more often than during the last months. I love you all.

Niclas Pettersson, Göteborg 2013

This work was founded by grants from the King Gustav V Jubilee Clinic Cancer Research Foundation, The Swedish Cancer Society, and The Swedish state under the ALF agreement.

7. REFERENCES

1. **Hall, E.J., Giacca, A.J.,** *Radiobiology for the Radiologist.* 6 ed. 2006, Philadelphia: Lippincott Williams & Wilkins.
2. **Jemal, A., et al.,** *Global cancer statistics.* CA Cancer J Clin, 2011. 61(2): p. 69-90.
3. **Verellen, D., M.D. Ridder, and G. Storme,** *A (short) history of image-guided radiotherapy.* Radiotherapy and Oncology, 2008. 86(1): p. 4-13.
4. **Thames, H.D., Hendry, J.H.,** *Fractionation in Radiotherapy.* 1987, Basingstoke, Great Britain: Taylor & Francis.
5. **Barendsen, G.W.,** *Dose fractionation, dose rate and iso-effect relationships for normal tissue responses.* Int J Radiat Oncol Biol Phys, 1982. 8(11): p. 1981-97.
6. **Douglas, B.G. and J.F. Fowler,** *Letter: Fractionation schedules and a quadratic dose-effect relationship.* Br J Radiol, 1975. 48(570): p. 502-4.
7. **Thames, H.D., Jr., et al.,** *Changes in early and late radiation responses with altered dose fractionation: implications for dose-survival relationships.* Int J Radiat Oncol Biol Phys, 1982. 8(2): p. 219-26.
8. **Fowler, J.F.,** *The first James Kirk memorial lecture. What next in fractionated radiotherapy?* Br J Cancer Suppl, 1984. 6: p. 285-300.
9. **Fowler, J.F.,** *The linear-quadratic formula and progress in fractionated radiotherapy.* Br J Radiol, 1989. 62(740): p. 679-94.
10. **Withers, H.R., J.M. Taylor, and B. Maciejewski,** *The hazard of accelerated tumor clonogen repopulation during radiotherapy.* Acta Oncol, 1988. 27(2): p. 131-46.
11. **Bentzen, S.M.,** *Radiobiological considerations in the design of clinical trials.* Radiotherapy and Oncology, 1994. 32(1): p. 1-11.
12. **Pop, L.A., et al.,** *Constraints in the use of repair half times and mathematical modelling for the clinical application of HDR and PDR treatment schedules as an alternative for LDR brachytherapy.* Radiother Oncol, 1996. 38(2): p. 153-62.
13. **Park, C., et al.,** *Universal survival curve and single fraction equivalent dose: useful tools in understanding potency of ablative radiotherapy.* Int J Radiat Oncol Biol Phys, 2008. 70(3): p. 847-52.
14. **Astrahan, M.,** *Some implications of linear-quadratic-linear radiation dose-response with regard to hypofractionation.* Medical physics, 2008. 35: p. 4161.
15. **Brenner, D.J.** *The linear-quadratic model is an appropriate methodology for determining isoeffective doses at large doses per fraction.* in Seminars in radiation oncology. 2008. Elsevier.
16. **Guerrero, M. and X.A. Li,** *Extending the linear–quadratic model for large fraction doses pertinent to stereotactic radiotherapy.* Physics in medicine and biology, 2004. 49(20): p. 4825.
17. **Fowler, J.F.,** *Linear quadratics is alive and well: In regard to Park et al.* Int J Radiat Oncol Biol Phys, 2008. 72(3): p. 957.
18. **Park, C., L. Papiez, and R.D. Timmerman,** *In reply to Dr. Fowler and Dr. Kavanagh.* Int J Radiat Oncol Biol Phys, 2008. 72(3): p. 958.
19. **Jackson, A., et al.,** *The lessons of QUANTEC: recommendations for reporting and gathering data on dose-volume dependencies of treatment outcome.* Int J Radiat Oncol Biol Phys, 2010. 76(3 Suppl): p. S155-60.
20. **Emami, B., et al.,** *Tolerance of normal tissue to therapeutic irradiation.* Int J Radiat Oncol Biol Phys, 1991. 21(1): p. 109-22.
21. **Burman, C., et al.,** *Fitting of normal tissue tolerance data to an analytic function.* Int J Radiat Oncol Biol Phys, 1991. 21(1): p. 123-35.
22. **Kutcher, G.J., et al.,** *Histogram reduction method for calculating complication probabilities for three-dimensional treatment planning evaluations.* Int J Radiat Oncol Biol Phys, 1991. 21(1): p. 137-46.
23. **Kallman, P., A. Agren, and A. Brahme,** *Tumour and normal tissue responses to fractionated non-uniform dose delivery.* Int J Radiat Biol, 1992. 62(2): p. 249-62.
24. **Jackson, A., G. Kutcher, and E. Yorke,** *Probability of radiation-induced complications for*

normal tissues with parallel architecture subject to non-uniform irradiation. Medical physics, 1993. 20(3): p. 613.

25. **Niemierko, A. and M. Goitein,** *Modeling of normal tissue response to radiation: the critical volume model.* Int J Radiat Oncol Biol Phys, 1993. 25(1): p. 135-45.

26. **Niemierko, A. and M. Goitein,** *Calculation of normal tissue complication probability and dose-volume histogram reduction schemes for tissues with a critical element architecture.* Radiother Oncol, 1991. 20(3): p. 166-76.

27. **Tucker, S.L., et al.,** *Dose-volume response analyses of late rectal bleeding after radiotherapy for prostate cancer.* Int J Radiat Oncol Biol Phys, 2004. 59(2): p. 353-65.

28. **Seppenwoolde, Y., et al.,** *Comparing different NTCP models that predict the incidence of radiation pneumonitis.* International Journal of Radiation Oncology* Biology* Physics, 2003. 55(3): p. 724-735.

29. **Wolbarst, A.B., L.M. Chin, and G.K. Svensson,** *Optimization of radiation therapy: integral-response of a model biological system.* International Journal of Radiation Oncology* Biology* Physics, 1982. 8(10): p. 1761-1769.

30. **Bentzen, S.M., et al.,** *Quantitative Analyses of Normal Tissue Effects in the Clinic (QUANTEC): an introduction to the scientific issues.* Int J Radiat Oncol Biol Phys, 2010. 76(3 Suppl): p. S3-9.

31. **Fletcher, G.H.,** *Hypofractionation: lessons from complications.* Radiotherapy and Oncology, 1991. 20(1): p. 10-15.

32. **Fletcher, G.H.,** *Regaud lecture perspectives on the history of radiotherapy.* Radiotherapy and oncology: journal of the European Society for Therapeutic Radiology and Oncology, 1988. 12(4): p. iii.

33. **Friberg, S. and B.I. Rudén,** *Hypofractionation in radiotherapy. An investigation of injured Swedish women, treated for cancer of the breast.* Acta Oncologica, 2009. 48(6): p. 822-831.

34. **Blomgren, H., et al.,** *Stereotactic high dose fraction radiation therapy of extracranial tumors using an accelerator: clinical experience of the first thirty-one patients.* Acta Oncologica, 1995. 34(6): p. 861-870.

35. **Arcangeli, S., M. Scorsetti, and F. Alongi,** *Will SBRT replace conventional radiotherapy in patients with low-intermediate risk prostate cancer? A review.* Critical reviews in oncology/hematology, 2012.

36. **Lax, I., et al.,** *Stereotactic radiotherapy of malignancies in the abdomen: methodological aspects.* Acta Oncologica, 1994. 33(6): p. 677-683.

37. **Kovacs, G., et al.,** *GEC/ESTRO-EAU recommendations on temporary brachytherapy using stepping sources for localised prostate cancer.* Radiother Oncol, 2005. 74(2): p. 137-48.

38. **Potter, R., et al.,** *Recommendations from gynaecological (GYN) GEC ESTRO working group (II): concepts and terms in 3D image-based treatment planning in cervix cancer brachytherapy-3D dose volume parameters and aspects of 3D image-based anatomy, radiation physics, radiobiology.* Radiother Oncol, 2006. 78(1): p. 67-77.

39. **Marks, L.B., R.K. Ten Haken, and M.K. Martel,** *Guest editor's introduction to QUANTEC: a users guide.* International Journal of Radiation Oncology* Biology* Physics, 2010. 76(3): p. S1-S2.

40. **Marks, L.B., et al.,** *Use of normal tissue complication probability models in the clinic.* International Journal of Radiation Oncology* Biology* Physics, 2010. 76(3): p. S10-S19.

41. **Steele, G.,** *Basic clinical radiobiology.* 3 ed. 2002, New York, NY, USA: Edward Arnold (Publishers) Ltd.

42. **Bentzen, S.M., et al.,** *Bioeffect modeling and equieffective dose concepts in radiation oncology–Terminology, quantities and units.* Radiotherapy and Oncology, 2012.

43. **Martinez, A., et al.,** *Conformal prostate brachytherapy: initial experience of a phase I/II dose-escalating trial.* Int J Radiat Oncol Biol Phys, 1995. 33(5): p. 1019.

44. **Trotti, A., et al.** *CTCAE v3. 0: development of a comprehensive grading system for the adverse effects of cancer treatment.* in Seminars in radiation oncology. 2003. Elsevier.

45. **Cox, J.D., J. Stetz, and T.F. Pajak,** *Toxicity criteria of the Radiation Therapy Oncology Group (RTOG) and the European Organization for Research and Treatment of Cancer (EORTC).* Int J Radiat Oncol Biol Phys, 1995. 31(5): p. 1341-6.

46. **Rubin, P., et al.,** *RTOG Late Effects Working Group. Overview. Late Effects of Normal Tissues (LENT) scoring system.* Int J Radiat Oncol Biol Phys, 1995. 31(5): p. 1041-2.

47. **Alsadius, D., et al.,** *Tobacco smoking and long-lasting symptoms from the bowel and the anal-sphincter region after radiotherapy for prostate cancer.* Radiotherapy and Oncology, 2011. 101(3): p. 495-501.

48. **Alsadius, D., et al.,** *Mean Absorbed Dose to the Anal-Sphincter Region and Fecal Leakage among Irradiated Prostate Cancer Survivors.* International Journal of Radiation Oncology* Biology* Physics, 2012.

49. **Steineck, G., et al.,** *Symptom documentation in cancer survivors as a basis for therapy modifications.* Acta Oncol, 2002. 41(3): p. 244-52.

50. **Steineck, G., H. Hunt, and J. Adolfsson,** *A hierarchical step-model for causation of bias-evaluating cancer treatment with epidemiological methods.* Acta Oncol, 2006. 45(4): p. 421-9.

51. **ICRU Report 83.** *Prescribing, recording, and reporting photon beam intensity-modulated radiation therapy (IMRT), International Commission on Radiation Units and Measurements.* 2010, Bethesda, MD, USA.

52. **ICRU Report 58.** *Dose and volume specification for reporting interstitial brachytherapy, International Commission on Radiation Units and Measurements.* 1997, Bethesda, MD, USA.

53. **Kutcher, G.J. and C. Burman,** *Calculation of complication probability factors for non-uniform normal tissue irradiation: the effective volume method.* Int J Radiat Oncol Biol Phys, 1989. 16(6): p. 1623-30.

54. **Lyman, J.T.,** *Complication probability as assessed from dose-volume histograms.* Radiat Res Suppl, 1985. 8: p. S13-9.

55. **Niemierko, A.,** *A generalized concept of equivalent uniform dose (EUD) (Abstract).* Med Phys, 1999. 26: p. 1100.

56. **Bentzen, S.M.,** *Steepness of the radiation dose-response curve for dose-per-fraction escalation keeping the number of fractions fixed.* Acta Oncol, 2005. 44(8): p. 825-8.

57. **Bentzen, S.M. and S.L. Tucker,** *Quantifying the position and steepness of radiation dose-response curves.* Int J Radiat Biol, 1997. 71(5): p. 531-42.

58. **Brahme, A.,** *Dosimetric precision requirements in radiation therapy.* Acta Radiol Oncol, 1984. 23(5): p. 379-91.

59. **Borst, G.R., et al.,** *Radiation pneumonitis after hypofractionated radiotherapy: evaluation of the LQ (L) model and different dose parameters.* International Journal of Radiation Oncology* Biology* Physics, 2010. 77(5): p. 1596-1603.

60. **Olsson, C. and K.A. Johansson,** *Do we need fractionation-corrected doses in sequential two-phase treatments? A quantification of dose differences between non-corrected and corrected combined non-uniform dose distributions in normal tissue.* Acta Oncologica, 2010. 49(8): p. 1253-1260.

61. **Tucker, S.L., et al.,** *Analysis of radiation pneumonitis risk using a generalized Lyman model.* Int J Radiat Oncol Biol Phys, 2008. 72(2): p. 568-74.

62. **El Naqa, I., et al.,** *Multivariable modeling of radiotherapy outcomes, including dose–volume and clinical factors.* International Journal of Radiation Oncology* Biology* Physics, 2006. 64(4): p. 1275-1286.

63. **Pawitan, Y.,** *In all likelihood: Statistical Modelling and Inference Using Likelihood.* Oxford: Clarendon. 2001.

64. **Schilstra, C. and H. Meertens,** *Calculation of the uncertainty in complication probability for various dose-response models, applied to the parotid gland.* Int J Radiat Oncol Biol Phys, 2001. 50(1): p. 147-58.

65. **Gagliardi, G., et al.,** *Radiation pneumonitis after breast cancer irradiation: analysis of the complication probability using the relative seriality model.* Int J Radiat Oncol Biol Phys, 2000. 46(2): p. 373.

66. **Lind, P.A., et al.,** *ROC curves and evaluation of radiation-induced pulmonary toxicity in breast cancer.* Int J Radiat Oncol Biol Phys, 2006. 64(3): p. 765-70.

67. **Metz, C.E.,** *Basic principles of ROC analysis.* Semin Nucl Med, 1978. 8(4): p. 283-98.

68. **Metz, C.E.,** *ROC methodology in radiologic imaging.* Invest Radiol, 1986. 21(9): p. 720-33.

69. **Socialstyrelsen.** *Cancerstatistik. 2013-02-01;* Available from: http://192.137.163.49/sdb/can/val.aspx.

70. **Socialstyrelsen.** *Dödsorsaksstatistik. 2013-02-01;* Available from: http://192.137.163.49/sdb/dor/val.aspx.

71. **Thun, M.J., et al.,** *Lung cancer occurrence in never-smokers: an analysis of 13 cohorts and 22 cancer registry studies.* PLoS medicine, 2008. 5(9): p. e185.

72. **Cancer.org.** *2013-02-09;* Available from: http://www.cancer.org/cancer/lungcancer-non-small-cell/detailedguide/non-small-cell-lung-cancer-survival-rates.

73. **Qiao, X., et al.,** *The role of radiotherapy in treatment of stage I non-small cell lung cancer.* Lung Cancer, 2003. 41(1): p. 1-11.

74. **Chi, A., et al.,** *Stereotactic Body Radiation Therapy in Non–Small-Cell Lung Cancer: Linking Radiobiological Modeling and Clinical Outcome.* American Journal of Clinical Oncology, 2011. 34(4): p. 432-441.

75. **Hayman, J.A., et al.,** *Dose escalation in non–small-cell lung cancer using three-dimensional conformal radiation therapy: Update of a phase I trial.* Journal of clinical oncology, 2001. 19(1): p. 127-136.

76. **Martel, M.K., et al.,** *Estimation of tumor control probability model parameters from 3-D dose distributions of non-small cell lung cancer patients.* Lung Cancer, 1999. 24(1): p. 31-37.

77. **Fowler, J.F., et al.,** *A challenge to traditional radiation oncology.* International Journal of Radiation Oncology* Biology* Physics, 2004. 60(4): p. 1241-1256.

78. **Nyman, J., K.A. Johansson, and U. Hulten,** *Stereotactic hypofractionated radiotherapy for stage I non-small cell lung cancer—mature results for medically inoperable patients.* Lung Cancer, 2006. 51(1): p. 97-103.

79. **Hanks, G., K. Martz, and J. Diamond,** *The effect of dose on local control of prostate cancer.* International Journal of Radiation Oncology* Biology* Physics, 1988. 15(6): p. 1299-1305.

80. **Dearnaley, D.P., et al.,** *Comparison of radiation side-effects of conformal and conventional radiotherapy in prostate cancer: a randomised trial.* The Lancet, 1999. 353(9149): p. 267-272.

81. **Ten Haken, R., et al.,** *Boost treatment of the prostate using shaped, fixed fields.* International Journal of Radiation Oncology* Biology* Physics, 1989. 16(1): p. 193-200.

82. **Wong, J.R., et al.,** *Image-guided radiotherapy for prostate cancer by CT–linear accelerator combination: Prostate movements and dosimetric considerations.* International Journal of Radiation Oncology* Biology* Physics, 2005. 61(2): p. 561-569.

83. **Kovacs, G., et al.,** *Improvement of interstitial brachytherapy for localized prostate neoplasms with a new implantation technique.* German Strahlenther Onkol, 1995. 171: p. 685-8.

84. **Kovács, G., et al.,** *Prostate preservation by combined external beam and HDR brachytherapy in nodal negative prostate cancer.* Strahlentherapie und Onkologie, 1999. 175: p. 87-88.

85. **Brenner, D.J. and E.J. Hall,** *Fractionation and protraction for radiotherapy of prostate carcinoma.* International Journal of Radiation Oncology* Biology* Physics, 1999. 43(5): p. 1095-1101.

86. **Miralbell, R., et al.,** *Dose-Fractionation Sensitivity of Prostate Cancer Deduced From Radiotherapy Outcomes of 5,969 Patients in Seven International Institutional Datasets: α/β= 1.4 (0.9–2.2) Gy.* International Journal of Radiation Oncology* Biology* Physics, 2012. 82(1): p. e17-e24.

87. **Pedicini, P., L. Strigari, and M. Benassi,** *Estimation of a Self-Consistent Set of Radiobiological Parameters From Hypofractionated Versus Standard Radiation Therapy of Prostate Cancer.* Int J Radiat Oncol Biol Phys, 2013.

88. **Dasu, A. and I. Toma-Dasu,** *Impact of variable RBE on proton fractionation.* Medical physics, 2013. 40: p. 011705.

89. **Fowler, J.F., et al.,** *What hypofractionated protocols should be tested for prostate cancer?* Int J Radiat Oncol Biol Phys, 2003. 56(4): p. 1093-1104.

90. **Borghede, G., et al.,** *Irradiation of localized prostatic carcinoma with a combination of high dose rate iridium-192 brachytherapy and external beam radiotherapy with three target definitions and dose levels inside the prostate gland.* Radiother Oncol, 1997. 44(3): p. 245-50.

91. **Borghede, G., et al.,** *Combined treatment with temporary short-term high dose rate iridium-192 brachytherapy and external beam radiotherapy for irradiation of localized prostatic carcinoma.* Radiotherapy and Oncology, 1997. 44(3): p. 237-244.

92. **Viswanathan, A.N., et al.,** *Radiation dose-volume effects of the urinary bladder.* Int J Radiat Oncol Biol Phys, 2010. 76(3 Suppl): p. S116-22.

93. **Goldner, G., et al.,** *Acute side effects during 3-D-planned conformal radiotherapy of prostate cancer.* Strahlentherapie und Onkologie, 2003. 179(5): p. 320-327.

94. **Talcott, J.A., et al.,** *Patient-reported symptoms after primary therapy for early prostate cancer: results of a prospective cohort study.* Journal of clinical oncology, 1998. 16(1): p. 275-283.

95. **Asai, K., et al.,** *Radiation-Induced Rib Fractures After Hypofractionated Stereotactic Body Radiation Therapy: Risk Factors and Dose–Volume Relationship.* International Journal of Radiation Oncology* Biology* Physics, 2012.

96. **Kanemoto, A., et al.,** *Dose-volume histogram analysis for risk factors of radiation-induced rib fracture after hypofractionated proton beam therapy for hepatocellular carcinoma.* Acta Oncologica, 2012(0): p. 1-7.

97. **Kim, S.S., et al.,** *Clinical prognostic factors and grading system for rib fracture following stereotactic body radiation therapy (SBRT) in patients with peripheral lung tumors.* Lung Cancer, 2012.

98. **Fogliata, A., et al.,** *On the dosimetric behaviour of photon dose calculation algorithms in the presence of simple geometric heterogeneities: comparison with Monte Carlo calculations.* Phys Med Biol, 2007. 52(5): p. 1363-85.

99. **Knoos, T., et al.,** *Comparison of dose calculation algorithms for treatment planning in external photon beam therapy for clinical situations.* Phys Med Biol, 2006. 51(22): p. 5785-807.

100. **Lax, I., et al.,** *Dose distributions in SBRT of lung tumors: Comparison between two different treatment planning algorithms and Monte-Carlo simulation including breathing motions.* Acta Oncol, 2006. 45(7): p. 978-88.

101. **Siebers, J., et al.,** *Converting absorbed dose to medium to absorbed dose to water for Monte Carlo based photon beam dose calculations.* Physics in medicine and biology, 2000. 45(4): p. 983.

102. **Peeters, S.T.H., et al.,** *Acute and late complications after radiotherapy for prostate cancer: results of a multicenter randomized trial comparing 68 Gy to 78 Gy.* International Journal of Radiation Oncology Biology Physics, 2005. 61(4): p. 1019-1034.

103. **Adolfsson, J., et al.,** *Urinary and bowel symptoms in men with and without prostate cancer: results from an observational study in the Stockholm area.* European urology, 1998. 33(1): p. 11-16.

104. **Mirza, M., T.L. Griebling, and M.W. Kazer.** *Erectile Dysfunction and Urinary Incontinence After Prostate Cancer Treatment.* in Seminars in Oncology Nursing. 2011. Elsevier.

105. **Parsons, B.A., S. Evans, and M.P. Wright,** *Prostate cancer and urinary incontinence.* Matrix Biology, 2009. 63(4): p. 323-328.

106. **Schmid, M.P., et al.,** *Late gastrointestinal and urogenital side-effects after radiotherapy–Incidence and prevalence. Subgroup-analysis within the prospective Austrian–German phase II multicenter trial for localized prostate cancer.* Radiotherapy and Oncology, 2012.

107. **Moinpour, C.M., et al.,** *Health-related quality of life results in pathologic stage C prostate cancer from a Southwest Oncology Group trial comparing radical prostatectomy alone with radical prostatectomy plus radiation therapy.* Journal of clinical oncology, 2008. 26(1): p. 112-120.

108. **Potosky, A.L., et al.,** *Five-year outcomes after prostatectomy or radiotherapy for prostate cancer: the prostate cancer outcomes study.* Journal of the National Cancer Institute, 2004. 96(18): p. 1358-1367.

109. **Fransson, P.,** *Patient-reported lower urinary tract symptoms, urinary incontinence, and quality of life after external beam radiotherapy for localized prostate cancer-15 years' follow-up. A comparison with age-matched controls.* Acta Oncologica, 2008. 47(5): p. 852-861.

110. **Duchesne, G.M., et al.,** *Patterns of toxicity following high-dose-rate brachytherapy boost for prostate cancer: mature prospective phase I/II study results.* Radiotherapy and Oncology, 2007. 84(2): p. 128-134.